NANO · MICRO small
www.small-journal.com

DNAzyme-Functionalized Nanomaterials: Recent Preparation, Current Applications, and Future Challenges

*Jabrane Jouha and Hai Xiong**

DNAzyme–nanomaterial bioconjugates are a popular hybrid and have received major attention for diverse biomedical applications, such as bioimaging, biosensor development, cancer therapy, and drug delivery. Therefore, significant efforts are made to develop different strategies for the preparation of inorganic and organic nanoparticles (NPs) with specific morphologies and properties. DNAzymes functionalized with metal–organic frameworks (MOFs), gold nanoparticles (AuNPs), graphene oxide (GO), and molybdenum disulfide (MoS_2) are introduced and summarized in detail in this review. Moreover, the focus is on representative examples of applications of DNAzyme–nanomaterials over recent years, especially in bioimaging, biosensing, phototherapy, and stimulation response delivery in living systems, with their several advantages and drawbacks. Finally, the perspective regarding the future directions of research addressing these challenges is also discussed and highlighted.

1. Introduction

DNAzymes are single-stranded DNA (ssDNA) molecules that can catalyze a variety of reactions, such as RNA and DNA ligation or cleavage, and so on. DNAzymes have also have been widely exploited as potential therapeutic agents for gene silencing and inclusion in biosensing platforms because of their unique cofactor-dependent and sequence-specific catalytic properties.[1–5] However, most of the reported DNAzyme-based sensors utilize RNA-cleaving DNAzymes (RCD) discovered in 1994 by the Joyce group.[6] A representative DNAzyme for RNA cleavage shares a similar secondary structure with two binding arms and an active site in the middle.[7] In addition, the transition state takes places where the 2′-OH group, next to the scissile phosphodiester, in the ribo-adenine (rA) serves a nucleophile to displace the 5′-oxygen in the phosphodiester, resulting in two cleavage fragments with a 2′–3′ cyclic phosphate and a 5′-OH terminus supported by metal ions.[8,9] Of all types of DNAzymes, 8–17 and 10–23 DNAzymes are the two most popular ones because they can cleave the phosphodiester bonds between any unpaired purine–pyrimidine.[10,11] In the presence of specific metal ions such as Mg^{2+},[12] Pb^{2+},[13] Cu^{2+},[14] and Na^{+},[15,16] DNAzyme can successfully cut off the target messenger RNA (mRNA) by catalyzing the hydrolysis of the phosphodiester of target RNA. Another important DNAzyme used is the G-quadruplex/hemin peroxidase-mimicking DNAzyme. Assisted by a hemin cofactor, which can catalyze an oxidation reaction between H_2O_2 and chromogenic substrates, such as 2,2′-azinobis (3-ethylbenzothiazoline-6-sulfonic acid) (ABTS) and 3,3′,5,5′-tetramethylbenzidine (TMB), producing a signal amplification.[17–19] In fact, many researches on DNAzymes have been reviewed elsewhere.[20–24]

Metal–organic frameworks (MOFs) are promising next-generation materials for a wide range of applications, including selective catalysis,[25–30] conductivity material for fuel cells,[31,32] gas adsorption and purification,[33–36] sensing,[37–40] drug delivery, and biomedical applications including photodynamic/photothermal therapy (PDT).[41–44] Their high ability to modify porosity and large surface area improves the controlled release of several biological substances, features ease of functionalization, good water solubility, degradability, and biocompatibility. Furthermore, MOFs are created as robust solid systems for anchoring oligonucleotides via adsorption[45,46] and van der Waals (vdW) interactions,[47] or covalent conjugation.[48,49] Because of these properties and the inherent chemistry of MOFs, they can also encapsulate biocomposites based on living cells and viruses as well as bio-macromolecules (e.g., enzymes, proteins, polysaccharides, and DNA).[50–52]

Benefiting from their chemical stability, unique optical and electronic features, low-/non-cytotoxicity, high surface-to-volume ratio, and easy synthesis with different sizes and shapes, gold nanoparticles (AuNPs) show potential applications in nanoscience,[53,54] photocatalysts,[55] chemical and biological sensing,[56,57] and as theranostic platforms.[58–61] Recently, the roles of stabilizing agents, such as surfactants, polymers, silica, polyethylene glycol (PEG) ligands, and metal shells in colloidal suspensions of AuNPs, were reported.[62] In particular, AuNPs have been extensively exploited to construct functionalized nanoplatforms with a wide variety of biomolecules including enzymes,[63,64] antibodies,[65,66] peptides or protein,[67–69] and nucleic acids,[70–73] which attracted immense attention as sensors, for bioimaging, drug delivery, and even clinical treatment.[74]

J. Jouha, H. Xiong
Institute for Advanced Study
Shenzhen University
Shenzhen 518060, China
E-mail: hai.xiong@szu.edu.cn
J. Jouha
College of Physics and Optoelectronic Engineering
Shenzhen University
Shenzhen 518060, China

The ORCID identification number(s) for the author(s) of this article can be found under https://doi.org/10.1002/smll.202105439.

DOI: 10.1002/smll.202105439

2D materials are promising building blocks for advanced biomedical applications, due to their unique physical, robust mechanical, and chemical properties.[75–77] Mostly, graphene oxide (GO) and molybdenum disulfide (MoS_2) have been the subject of various researches. Furthermore, these nanoparticles can be generated on a large scale and exhibit intense fluorescence properties in aqueous solutions, and the use of these two materials for DNA-based detection has been developed with simple DNA[78–81] and aptamers.[82,83]

Among the diverse combinations of biomolecules and nanomaterials, DNA-functionalized inorganic surfaces including metal–organic frameworks, gold nanoparticles, carbon-based nanomaterials, and metal oxides have provided one of the most versatile hybrid platforms.[72,84–88] These materials can achieve optical signals, act as transport vehicles, and deliver metal ions for DNAzyme catalysis. Recently, several reviews concerning the design and application of DNAzymes or the biological applications of nanomaterials have been published.[89–92] However, a few reviews have focused on current advances (especially within the last few years) and future challenges involving DNAzyme nanomaterials, which might be important for advancements in the field.

Herein, we will focus on summarizing relevant examples of the encapsulation of DNAzymes in MOF shells, AuNPs, GO, or MoS_2, with wide ranging applications in various fields such as drug delivery, biosensing, and imaging cells. Furthermore, we conclude with their perspectives on biomedical applications and the future directions that might be the focus of further study.

2. Preparation of DNAzyme@nanomaterials

Different strategies are available for the preparation of the DNA conjugates based on nanomaterials. Unlike the typical ssDNA or double-stranded DNA (dsDNA), DNA/RNA cleaving DNAzymes have single- and double-stranded sections, and exhibit a variety of secondary structures. The bases of the rigid duplex regions are protected, whereas the ssDNA regions are more pliable and can be better conjugated to surfaces. In addition, the structure of DNA and the lengths of nucleobases strongly influence the interactions between DNA and nanomaterials. To construct advanced DNAzyme–nanomaterial platforms, herein we describe the most successful methods employing DNA and nanomaterials as building elements.

2.1. DNAzyme@MOFs

Nucleic acids are well known for their fragile nature and their digestion by nucleases. Thus, searching for potential vectors able to absorb and release these molecules remains a challenge. MOFs can afford promising nonviral vectors for the cellular transmission of plasmid DNA.[93] The first example of nucleic acid–MOF nanoparticle hybrids was reported by Mirkin and co-workers in 2014. Using a strain-promoted click reaction, the oligonucleotides with a dibenzylcyclooctyne were added to an azide-functionalized UiO-66 MOF. Compared to nonfunctionalized MOF particles, UiO-66 MOFs made a steric and electrostatic barrier, which increased stability and enhanced cellular ingestion capacities.[43]

Similarly, Zhou et al. have used the reversible DNA infiltration into the pores of MOFs. The diverse lengths (11–53 bp) of ssDNA can be selectively bound into a class of MOFs (Ni-IRMOF-74-II–V). This provides precise release of ssDNA with high transfection efficiency into a wide range of cell types such as $CD4^+$ T and THP-1 cells, and unmatched by the commercialized nonviral vectors including Neofect and Lipo (50%) as shown in **Figure 1**a and Figure 1b, respectively.[47] The Shukla group has also explored a facile synthetic method suitable for encapsulating the plasmid DNA (pDNA) of MOF vectors for intracellular gene delivery. In the presence of propidium iodide (PI), pDNA-encapsulating zeolitic imidazole framework-8 (ZIF-8) has a peak at 617 nm, and represents a fluorescent DNA stain commonly used for staining cellular DNA (Figure 1c–f). Moreover, the encapsulated green fluorescent protein (GFP) plasmid (plGFP) remained almost intact due to the detection of green fluorescent signals for GFP expression in human prostate cancer epithelial cells (PC-3).[94] To encapsulate pDNA into ZIF-8, Tang's group used a similar approach but followed a one-pot method via biomimetic mineralization and coprecipitation.[93] Benefiting from their protection against nuclease activity, the pDNA molecules are very well shared within the two nanostructures. Additionally, plGFP-C1@ZIF-8-PEI nanosheets exhibit great pH-responsive, better loading capacity and solid binding affinity owing to the higher electrostatic interaction between polyethyleneimine (PEI) and pDNA (Figure 1g). In vitro tests showed that the ZIF-8-PEI 25 kD vector improves cellular uptake and endosomal escape of the protected pDNA, resulting in effective gene expression with high transfection efficacy. To achieve gene silencing of the human early growth response-1 (EGR-1) mRNA and its cleavage activity, the ZIF-8 produced DNAzyme and Zn^{2+} ions once within the cells. In further investigations, a functionalized DNAzyme with a chlorin e6 moiety was encapsulated in ZIF-8 nanoparticles.[95] For photodynamic therapy, the auxiliary photosensitizer (PS) Ce6 can induce reactive oxygen species (ROS) in cancer cells, leading to a reduction in tumor size. This nanosystem could successfully be delivered a therapeutic DNAzyme to cancer cells while avoiding nuclease kinetics.

Farha and co-workers also described a new approach for intracellular protein delivery that depends on the DNA–MOF system.[96] In this method, 74 NU-1000 and PCN-222/MOF-545 were produced in nanoparticle form to encapsulate insulin used as a model protein, as illustrated in Figure 1h–j. DNA layer was imposed to stabilize the function of the insulin-encapsulated MOF under high dielectric conditions, keeping the activity with a tenfold increase in cellular absorption. The good control over enzymatic degradation via advantageous DNA distribution on the periphery of insulin@MOF was attributed to the exceptional stability of the insulin-encapsulated, DNA-coated MOF. Currently, there is very little information about how cells interact with insulin-coated DNA-coated MOF nanoparticles during their absorption.

2.2. DNAzyme@AuNPs

The synthesis of DNAzyme–gold nanoparticles has received much attention in the development of new tools for potential applications. The interactions between DNA and AuNPs are

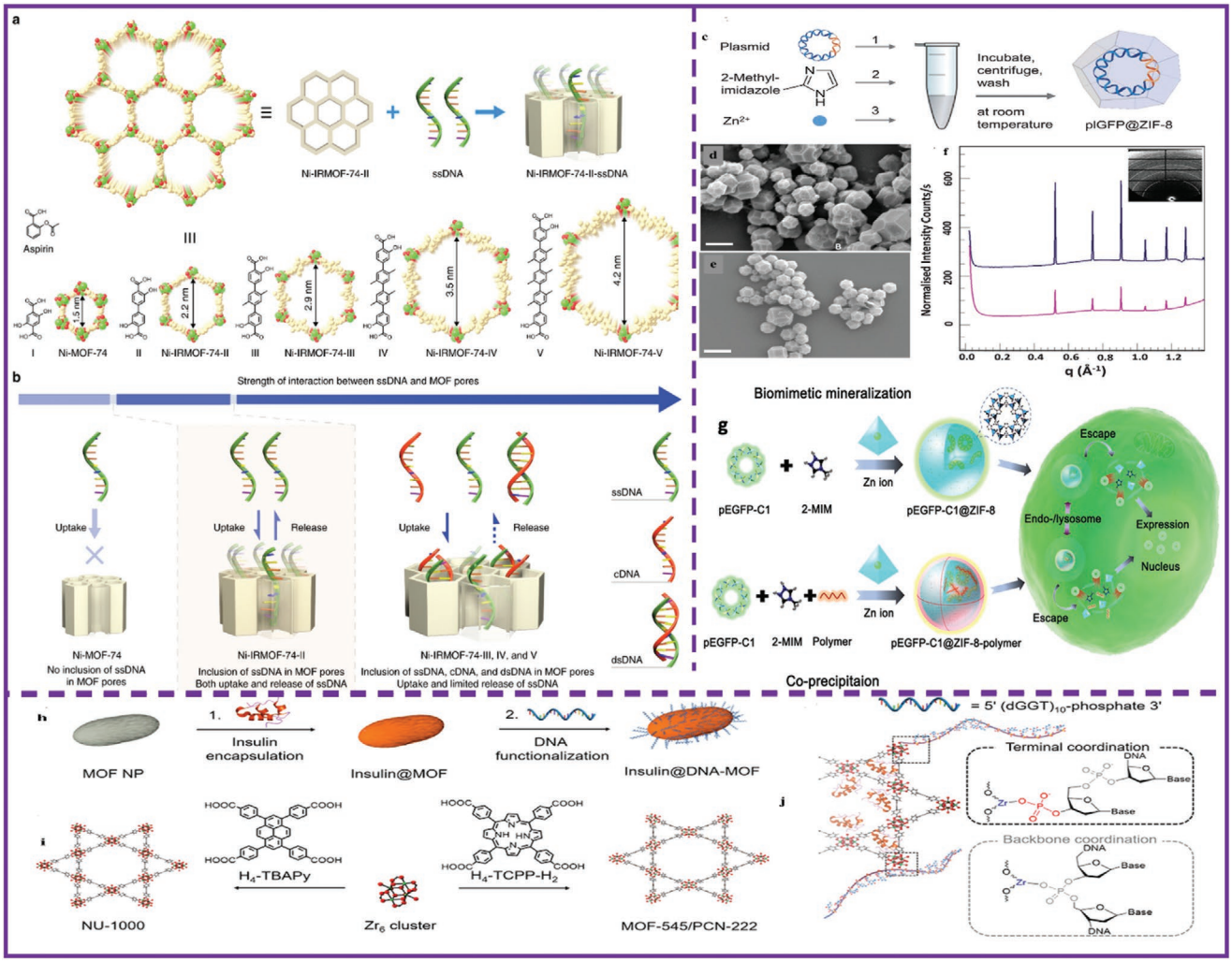

Figure 1. a) Schematic incorporation of ssDNA in Ni-IRMOF-74 series. b) Expression process: uptake, protection, and release of ssDNA using Ni-IRMOF-74-II. Adapted with permission.[47] Copyright 2018, Springer Nature. c) Schematic synthesis of plGFP@ZIF-8. Scanning electron microscopy image of d) ZIF-8 and e) plGFP@ZIF-8. f) Small-angle X-ray scattering (SAXS) patterns of ZIF-8 (black) and biomimetically mineralized plGFP@ ZIF-8 (purple) after the washing procedure. Adapted with permission.[94] Copyright 2019, Wiley-VCH. g) Schematic synthesis of pEGFP-C1@ZIF-8 through biomimetic mineralization and pEGFP-C1@ZIF-8-polymer applied coprecipitation method and their cellular uptake. Reproduced with permission.[93] Copyright 2019, Wiley-VCH. h) Schematic Illustration of insulin encapsulation MOF subsequently DNA surface functionalization. i) Crystal structures of two mesoporous Zr MOFs: NU-1000 and PCN-222/MOF-545, and their respective organic linkers. j) DNA functionalization of insulin encapsulated MOF NPs at 3′ terminal phosphate modified nucleic acids. Reproduced with permission.[96] Copyright 2019, American Chemical Society.

greatly influenced by the structure of DNA and the surface characteristics of AuNPs. Thiolated DNA with a high affinity for Au−S (200 kJ mol^{-1}) has long been applied to functionalize Au surfaces.[97–100] The negatively charged phosphate framework is not linked to the Au surface, but a phosphorothioate, in which sulfur substitutes one of the nonbridging oxygen atoms, has a higher affinity than DNA bases.[101] The higher reactivity between sulfur atoms and the surfaces of Au nanoparticles allows the construction of stable coordinated connections between Au and thiols. The original methodology used a salt-aging process, in which NaCl was progressively added to the system.[102,103] Mirkin et al. demonstrated that the salt is required to reduce their long-range charge repulsion so that DNA can be adsorbed onto AuNPs. As a result, the newly adsorbed DNA might push the adsorbed bases out of the way, forcing the DNAs to stand upright. In addition to charge screening, insertion of PEG between the amine/thiol functional group and the end of DNA molecules could improve DNA packing density by minimizing steric interactions and intermolecular repulsion of adjacent DNA strands at the surface of AuNPs.[104]

As classic examples, four construction methods including Au−S covalent conjugation,[102] Au adsorption,[105] electrostatic interactions,[106] and self-insertion[107] are summarized in **Figure 2**a–d. Unlike the Au−S covalent conjugation,[102] the coordination between the DNA bases and AuNPs is strong enough to fix DNA to the surface of gold nanomaterials (Figure 2b). Keto and imino groups on AuNPs can adsorb all four DNA bases.[108] According to numerous experimental studies, thymine has the lowest affinity, while adenine has the highest affinity, and the position of cytosine and guanine

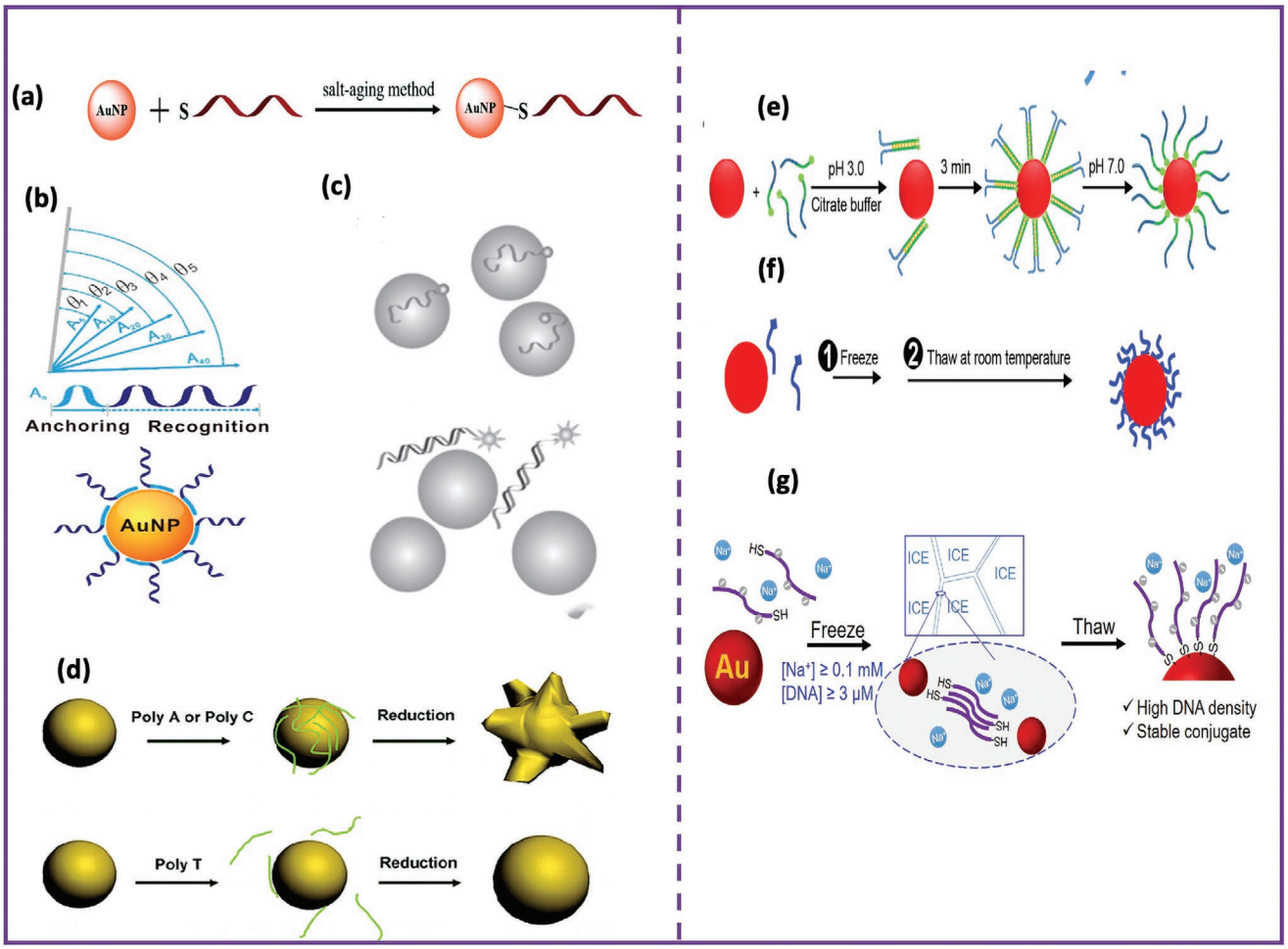

Figure 2. Interactions of gold nanoparticles and DNA: a) Au—S bond,[102] b) AuNPs–poly-A binding,[105] c) single strand adsorption interaction,[106] d) nucleic acid self-insertion interaction.[107] e) DNA containing poly-A at low pH is required to assemble into a parallel duplex.[117] f) The freezing operation requires no additional reagents.[117] g) Schematic showing freezing-directed conjugation of thiolated DNA onto AuNPs. Reproduced with permission.[118] Copyright 2019, American Chemical Society.

depending on the measurement.[105,109–111] Fan and co-workers designed monovalent or multivalent conjugates by combining ssDNA with poly-A. By altering the sequence length, and position of poly-A in the single strand, the valence bond may be tuned.[112,113] In the latter case, Lu and co-workers revealed a self-insertion approach for functionalization of DNA on the surface of gold nanoparticles, indicating that the affinity between DNA and AuNPs is essential for the deposition and diffusion of Au atoms as well as the morphological control of AuNPs.[107] Meanwhile, high-stability DNA functionalization was achieved in situ during the one-step synthesis while maintaining biorecognition, providing for the programmed assembly of novel nanostructures (Figure 2d). Due to the strong adsorption on the surface of spherical gold nanoparticles, poly-A and poly-C moderate the formation of flower-like gold nanoparticles, whereas poly-T retains the shape of spherical gold nanoparticles due to its poor adsorption. They also demonstrated that the DNA-functionalized nanoflowers are easily taken up by cells and can be observed under dark-field microscopy (DFM).

Using a low-pH buffer[114] or freezing,[115,116] Liu et al. developed methods that enabled quicker conjugation. In these studies, it was discovered that a high density of DNA could be achieved in 3 min at pH 3. DNA containing poly-A was later shown to be particularly appealing for this approach due to the production of parallel duplexes (Figure 2e).[117] An interesting approach was suggested by the same group who showed that DNA may be successfully connected by freezing and thawing mixtures of DNA and AuNPs without the need for any other reagents (Figure 2f).[115] More crucially, the DNA density was 20–30% higher than that obtained with traditional salt aging. DNA hybridization is also aided by lowering the temperature, enabling the creation of superior nanoflares with doubled probe density and signaling sensitivity. The ends of the DNA oligonucleotides can be aligned and stretched to expose them. The acidic and freezing conditions are still salt related, but the elongated conformation of DNA also has an important effect, allowing for substantially faster DNA adsorption while maintaining the upright orientation of DNA (Figure 2g).[116,118]

2.3. DNAzyme@MoS_2

MoS_2 is a form of transition metal sulfide that helps to improve planar electric transportation capabilities by stacking covalently bonded S—Mo—S through weak van der Waals interactions.[119] In comparison to other nanomaterials such as GO, MoS_2 nanosheets may be synthesized on a wide scale and have high fluorescence quenching characteristics in an aqueous solution for sensing without further processing. Furthermore, 2D-layered MoS_2 also exhibits better solubility in water, mechanical resistance, and electrical performance.[120] Moreover, the vdW forces are primarily responsible for the absorption of DNA by MoS_2 as a 2D-layered structure analogous to graphene, according to theoretical work shown in **Figure 3**.[121–123] This interaction between nucleobases and the basal plane of MoS_2 allows adsorption of ssDNA while rejecting dsDNA.[124,125]

By comparing their chemical structures, it is clear that MoS_2 is not the same as GO. For instance, GO can adsorb DNA by π–π stacking with DNA bases, but MoS_2 is nonaromatic. Fu's group was the first to report the binding of MoS_2 nanosheets with DNAzyme in 2015, and subsequently, the interaction of MoS_2 with DNA has been extensively studied.[80,119,126–129] Taking advantage of the fluorescence quenching potential (MoS_2) nanosheet and the specific recognition by DNAzyme, a novel fluorescent probe detection employing uranyl ion (UO_2^{2+}) in an aqueous environment has also been investigated.[130]

2.4. DNAzyme@GO

Because of their superior mechanical, electrical, and thermal properties, graphene-based sheets, particularly graphene oxide, have prompted a lot of interest in biological applications. Consequently, GO is an excellent fluorescence agent, tempering fluorescently labeled DNA almost completely upon adsorption. Furthermore, using π–π stacking and hydrogen bonding, the DNA fragments were released and adsorbed onto the GO surface. Therefore, ssDNA is more faster and effectively adsorbed by graphene oxide than dsDNA.[131] DNAzymes are the most common type of functional nucleic acids that can catalyze reactions or link to a target molecule, and they can recognize a wide range of targets. Investigation into the field of the interactions between GO and DNAzymes has been quite limited. For example, Wen et al. designed a Cy3-loaded substrate hybridized with the 17E DNAzyme, which has an insufficient affinity for binding to GO, while the cleavage substrate in the form of ssDNA was proficiently adsorbed.[132]

A few studies have been carried out regarding the interactions of GO and ssDNA strands with varying lengths of bases.[133,134] According to these studies, purine bases bind more firmly than pyrimidines, implying the importance of aromatic stacking. Furthermore, Min co-workers evaluated the DNA adsorption capacity and kinetics of two different sizes of GO using three different DNAs of various lengths.[135] They revealed that shorter DNA coated more efficiently into GO regardless of GO size, and that DNA had faster adsorption kinetics with nanographene oxide. Liu and co-workers demonstrated that poly-C DNA binds to GO much more strongly than other DNA homopolymers.[136] Using molecular dynamics simulations, it was found that enhanced phosphate backbone–GO hydrogen bonding was responsible for the increased poly-C affinity to GO at neutral pH.[137] The same group recently demonstrated that freezing DNA oligonucleotides stretched them and caused them to form more oxidized hydrophilic areas on GO.[138] Meanwhile, heating directed DNA to hydrophobic regions, leading to very stable conjugates that were more durable in terms of nonspecific displacement than the freezing samples as illustrated in **Figure 4**.

3. Current Applications

Nanomaterials possess optical and catalytic properties that enable to perform effectively the function of DNAzymes. Representative examples of applications of DNAzyme–nanomaterials in recent years, particularly in bioimaging biosensing, phototherapy, and stimulation response delivery in living cells have been discussed.

3.1. Applications of DNAzyme–MOF Nanoparticle Probes

Benefiting from their unique properties, such as chemical and structural adaptability, multiple coordination sites, large surface areas, and simple preparation, DNAzyme–MOF nanoparticle-based probes have been used in a variety of applications, including bioimaging and biosensing drug delivery, as well as phototherapy.

3.1.1. DNAzyme@MOF as Biosensing and Bioimaging Platforms

Following their successful preparation, DNAzyme@MOF-based probes have been used for biosensing and bioimaging of a variety of targets. These probes are divided into fluorescence

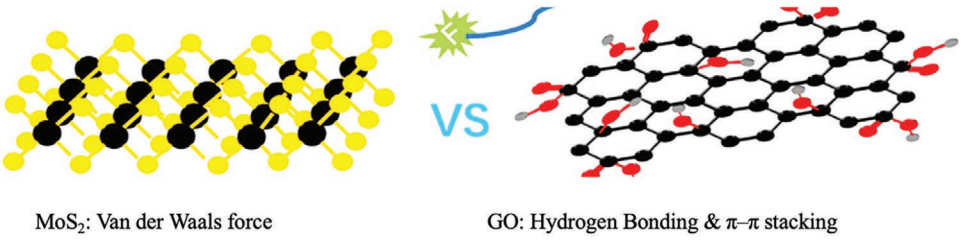

Figure 3. Schematic illustration of different interactions of DNA with MoS_2 and GO. Adapted with permission.[124] Copyright 2017, American Chemical Society.

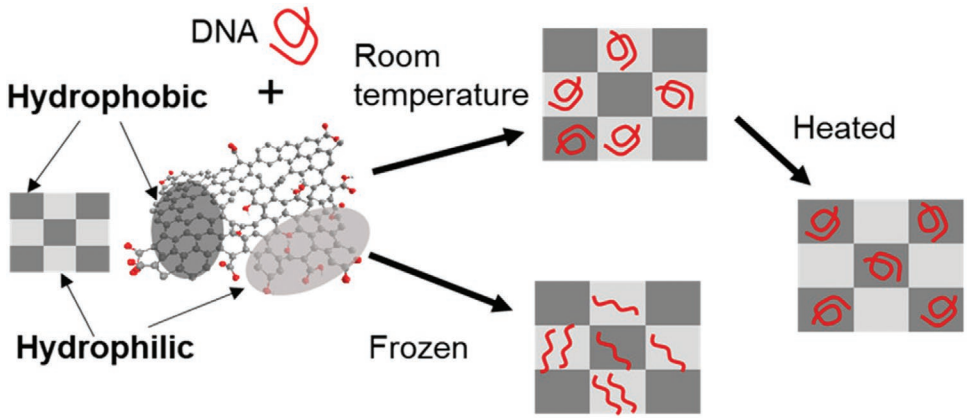

Figure 4. Schematic Illustration of the positions of DNA on GO and its operation mechanism depending on different conditions. Reproduced with permission.[138] Copyright 2020, American Chemical Society.

colorimetric, electrochemical, and photo-electrochemical sensors based on their output signals. A varies of probe sensing performances are presented in **Table 1**.

Fluorescence sensors show great promise for the identification of targets in vitro and living cells because of their great spatial resolution, high sensitivity, and quick detection speed. Detection and fluorescence imaging of intracellular molecules (including proteins, metal ions, and microRNAs (miRNAs)) can afford quantitative data concerning target expression levels, which is beneficial for biological research. Chu and co-workers prepared ZIF-8 as a potential carrier for a nucleic acid probe to access into cells, and a novel ratiometric fluorescence imaging approach using DNAzyme for miRNA-21 imaging was designed.[45] The 8–17 DNAzyme strand was labeled with a fluorophore (Cy5) at the 5′ terminus, and the substrate strand (S-DNA) was bonded with a fluorophore (Cy3) at the thymidine near the site of Cy5 having a segment complementary to the target miRNA-21 to produce a duplex probe (**Figure 5**a). The high level of Zn^{2+} on the ZIF-8 surface could attach an enormous number of nucleic acid probes via electrostatic coupling, protecting nucleic acids from cellular degradation and promoting endosome escape. With high contrast and repeatability, the proposed sensor was used to image miRNA-21 expression levels in MCF-7, HeLa, and L02 cells. Recently, Zhao and co-workers developed a ZIF-8-encapsulating DNAzyme nanoplatform by biomimetic mineralization.[139] ZIF-8, which is positively charged and has a high DNAzyme loading capacity, was able to penetrate cells. This biomimetic mineralization synthesis method provides more effective protection against DNase I activity, which is used as a model digesting enzyme, than free DNAzyme. This nanomaterial has allowed highly sensitive and selective fluorescent detection of Pb^{2+} in water, as well as Pb^{2+} bioimaging in living cells (Figure 5b,c). Moreover, the linear detection range for Pb^{2+} was $(50–500) \times 10^{-9}$ M.

Later, by immobilizing a Pb^{2+}-dependent DNAzyme onto a streptavidin-functionalized graphene oxide-tetraethylene pentamine-gold (rGO-TEPA-Au) nanoparticles platform, He and co-workers reported a highly sensitive and selective probe for the detection of Pb^{2+}.[140] The target catalytically cleaves the substrate strand of the DNAzyme in the presence of Pb^{2+}, causing the catalytic strand to separate from the sensor as shown in **Figure 6**a,b. The sensor's newly synthesized single-stranded DNA can hybridize with Fe–MOFs/PdPt NP-labeled hairpin DNA. The use of a Pb^{2+}-dependent DNAzyme improved selectivity of the biosensor, while Fe–MOFs/PdPt NPs-HP catalyzed H_2O_2 to amplify the electrochemical signal and improve sensitivity for the first time. Moreover, the biosensor was used to detect Pb^{2+} in water samples, with outstanding analytical performance for Pb^{2+}, showing that it has a lot of potential for environmental monitoring applications.

A further interesting example was described by Li and co-workers who reported two-photon (TP) imaging of Zn^{2+} in a living body using a phosphate-ion-activated DNAzyme MOF nanoprobe.[141] In this assay, a TP fluorophore at the 5′ end was coupled to the substrate-binding strand of the Zn^{2+}-specific DNAzyme (8–17), and the enzyme strand tagged with BHQ1 as a quencher. The double-stranded DNAzyme structure was initially formed by mixing these two strands simultaneously. Then, the assembly of TP–DNAzyme inside the MOFs was attributed mostly to the coordination between the DNAzyme backbone's phosphonate O atoms and Zr atoms in the MOFs, as shown in Figure 6c.

Because phosphate ions were present at high intracellular concentrations, the TP–DNAzyme was released from the surface of the MOFs. The substrate strand of the TP–DNAzyme is cleaved in the presence of Zn^{2+}, releasing a shorter DNA strand labeled with the TP fluorophore, resulting in a high fluorescence signal that might be clearly viewed with TP imaging. With a tissue signal penetration depth of 120 μm and

Table 1. The sensing performances of some typical sensors based on DNAzyme probes.

Sensors	Sensing performances	Ref.
Fluorescence sensors	Quick response, high sensitivity, high spatial resolution	[45,139]
Colorimetric sensor	Visualization of output signals, in situ and real-time detection, low cost	[161,164,165]
Electrochemical sensors	Quick response and high sensitivity, miniaturization and portability, low cost	[140]
Photo-electrochemical sensors	High sensitivity and low background noise	[171,178]

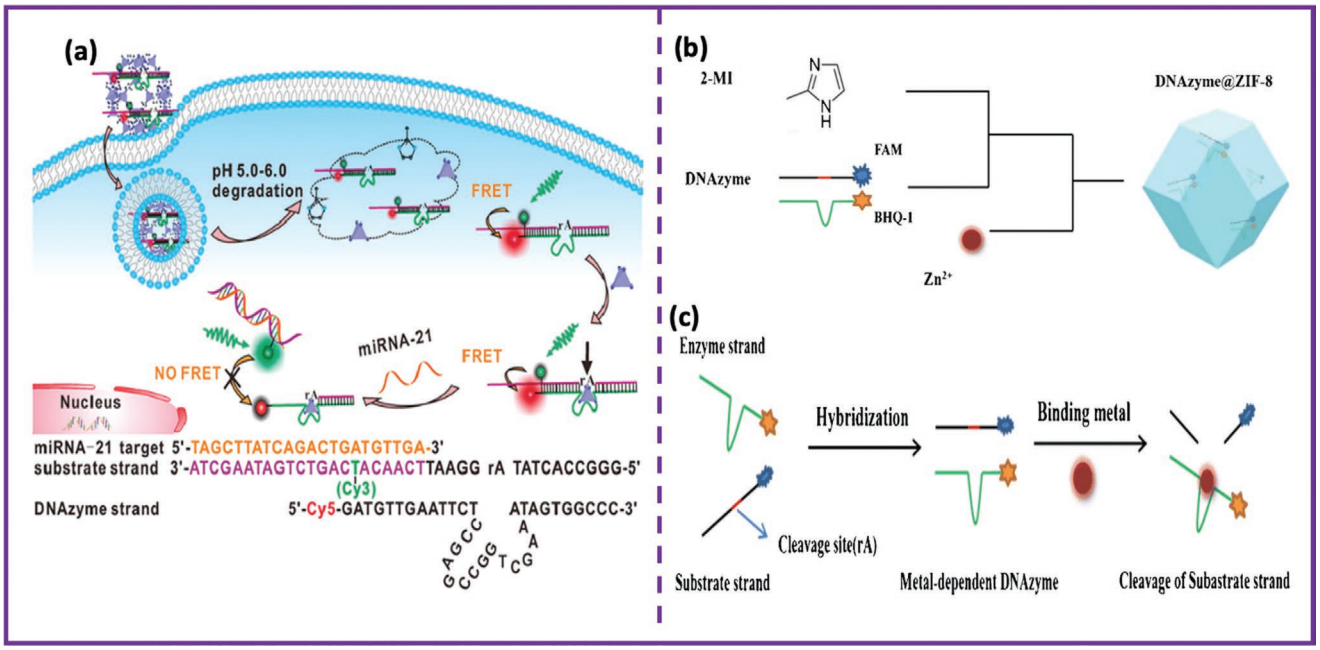

Figure 5. a) Sensing principle of the ratiometric fluorescence imaging strategy based on DNAzyme for miRNA-21 imaging. Reproduced with permission.[45] Copyright 2017, American Chemical Society. b) Schematic synthesis of DNAzyme@ZIF-8. c) Principle sensing of DNAzyme for metal ions' fluorescent detection. Reproduced with permission.[139] Copyright 2020, Springer.

a detection limit of 3.53×10^{-9} M, this TP–DNAzyme–MOF biosensor enables highly selective Zn^{2+} sensing and a tissue signal penetration of 120 m. This research also showed that the proposed sensor could be used to monitor apoptosis using Zn^{2+} determination and quantification.

3.1.2. DNAzyme@MOF Platform for Enhanced Phototherapy

Through electrostatic and coordination interactions, metal–organic frameworks can be used as flexible nanocarriers to accommodate functional nucleic acids such as DNAzymes.

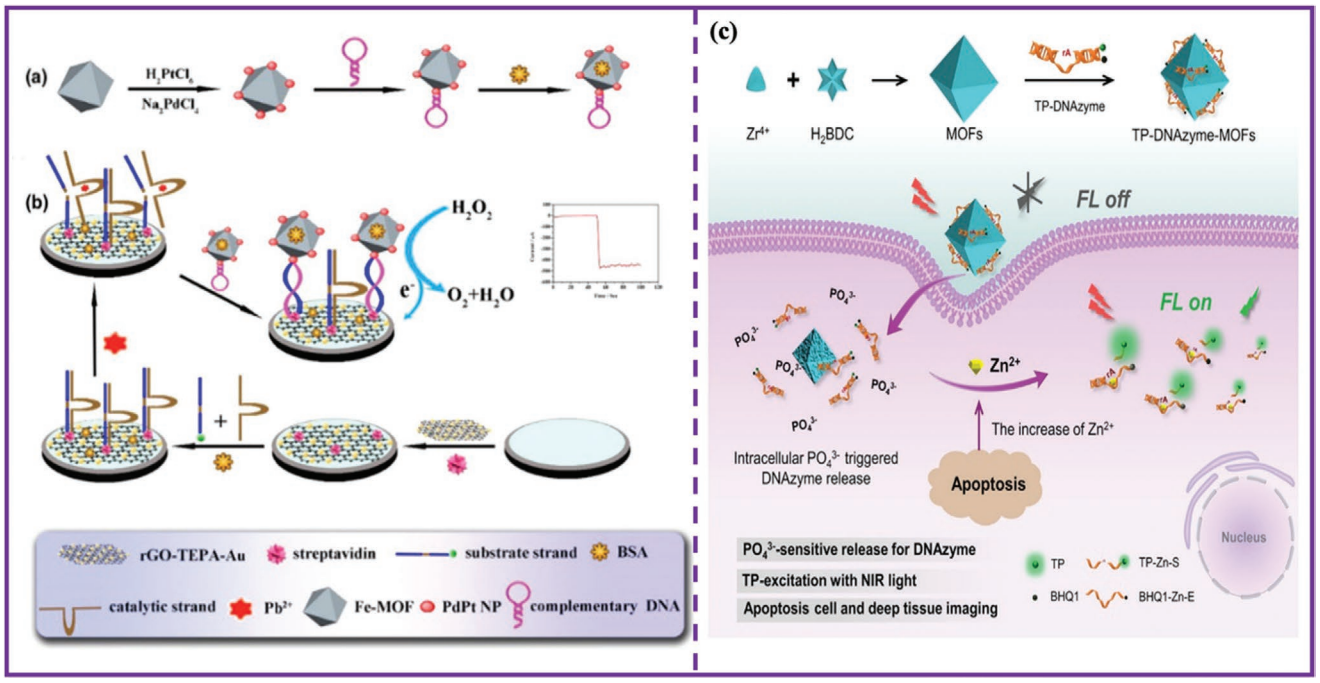

Figure 6. a) The preparation process of Fe-MOFs/PdPt NPs-HP. b) Schematic representation of the proposed strategy for the biosensor. Reproduced with permission.[140] Copyright 2018, Elsevier B.V. c) Design of the TP-DNAzyme–MOFs nanoprobe and Its functions in monitoring cell apoptosis. Reproduced with permission.[141] Copyright 2020, American Chemical Society.

Nowadays, MOFs are applied as an appropriate vehicle for delivering therapeutic payloads to cancer cells. Moreover, MOFs encapsulating DNAzyme/photosensitizer nanoplatforms might be constructed as a smart therapeutic nanosystem for much improved gene therapy owing to the auxiliary of photodynamic treatment. In this section, we review recent advancements in the use of DNAzyme@MOF-based nanoplatforms in cancer photodynamic treatment in this section, particularly the modification of MOFs based on their functions in PDT.

To date, Ce6 is a commercial PS used for fluorescence imaging-guided PDT, because of its near-infrared (NIR) fluorescence emission and capacity to produce significant quantities of ROS.[142,143] Poor solubility of Ce6 under physiological conditions,[144] which readily aggregates, poses several challenges, Ce6 fluorescence quenching in aggregation states results in lower PS activity or imaging signals. As a result, choosing appropriate vehicles to deliver Ce6 to tumor regions becomes crucial.

Wang et al. prepared a therapeutic nanosystem based on MOF-functionalized DNAzyme with a chlorin e6 and (Ce6D-NAzyme) for combined gene therapy and photodynamic treatment using one-pot encapsulation as shown in **Figure 7**a;[95] the rate of early apoptosis for the photoirradiated Ce6–DNAzyme@ZIF-8 grew to 44.9% after delivery into the acidic cytoplasm of cancer cells, which was significantly higher than with individual gene therapy or PDT, which only retained 19.85% and 33.6%, respectively (Figure 7b). After 21 days, the size and weight of

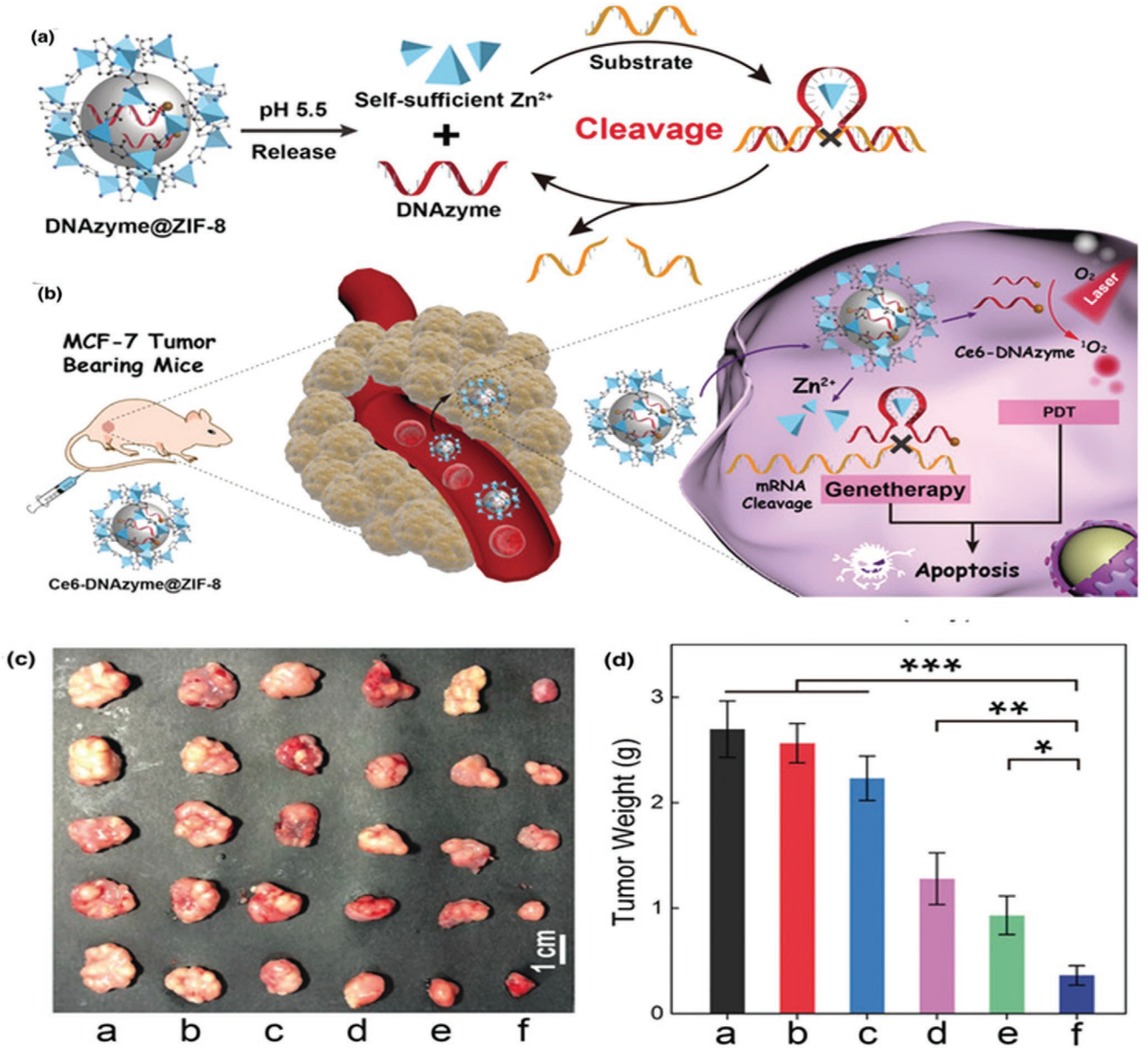

Figure 7. a)The pH-triggered release of DNAzyme and Zn^{2+}-ion cofactors for gene-silencing therapy. b) DNAzyme@ZIF-8 nanosystem for fluorescence imaging-guided combined gene/photodynamic therapy. c) Photographs and d) tumor weights after treatments with a) phosphate buffer saline, b) photoirradiation alone, c) Ce6-cDNA@ZIF-8, d) Ce6-DNAzyme@ZIF-8, e) photoirradiated Ce6-cDNA@ZIF-8, and f) the photoirradiated Ce6-DNAzyme@ZIF-8. Adapted with permission.[95] Copyright 2019, Wiley-VCH.

the tumors treated with "photoirradiated Ce6–DNAzyme@ZIF-8" (Figure 7c-e,f) and their controls (Figure 7c–a–e) were examined. The encapsulation technique prevents aggregation of Ce6, providing for effective imaging guidance using Ce6 fluorescence, whereas NIR-photoirradiated Ce6 produces singlet oxygen, allowing for an auxiliary phototherapeutic function.

3.1.3. Stimuli–Responsive Therapeutic Platform Based on DNAzyme@MOF

Stimuli–responsive-based metal–organic frameworks delivery backbones have attracted considerable interest in the controlled release of drugs and clinical treatment.[145–153] The stimuli for such reversible switching in these applications include exogenous stimuli (such as temperature, light, and pressure) and endogenous stimuli (such as pH, H_2S, glucose, ATP, and ions),[154] as illustrated in **Figure 8**.

Several publications have reported on the development of stimuli–responsive MOFs with chemical capping functions. However, the fabrication of stimuli–responsive DNAzyme/MOF hybrid platforms is rare and understudied. In addition, stimuli–responsive DNAzyme/MOF hybrids have been introduced as new functional materials for controlled drug release and nanomedical applications. The MOFs have the following benefits over the SiO_2 nanoparticles, which were reported previously:[155,156] i) MOFs have an ≈10-fold higher surface area than SiO_2 particles, allowing for precise nucleic acid–ligand modification; ii) nucleic-acid-functionalized MOFs are stable as mixtures in solution, whereas nucleic-acid-modified mesoporous SiO_2 nanoparticles tend to aggregate and precipitate; and iii) the coupling of nucleic acids to metal–organic frameworks as stimuli–responsive capping units is hugely interesting because biological components like genes, miRNA, or protein biomarkers might be employed to open the DNA caps. Willner and co-workers reported the first example of MOF loading and unloading using stimuli–responsive DNA-capping units. They developed a versatile strategy for covalently linking nucleic acids to nanoscale metal-organic framework (NMOFs) as stimuli–responsive carriers of pharmaceuticals or analogs of drugs, based on the "click chemistry" method.[48] Two distinct stimuli–responsive nucleic-acid-based NMOFs have been described. As a lock, one NMOF carrier used a pH-responsive nucleic acid duplex. The duplex DNA capping units were detached at pH = 5.0 by reconfiguration of the duplex constituents to the i-motif structure, allowing the capping units to be unlocked and the loads to be released. In the second system, NMOFs were labeled with doxorubicin (DOX) and using metal-ion-dependent substrate/DNAzyme complexes as stimuli–responsive nucleic acid capping units (metal ion: Mg^+ or Pb^+).

Nucleic acid locking units are split apart in the presence of the appropriate metal ions, leading to the release of cargo loads. Moreover, with the incorporation of the ATP aptamer sequence, "smart" Mg^{2+}-dependent DNAzyme-capped doxorubicin-loaded NMOFs were generated, as shown in Figure 10. The cooperative triggers including ATP and Mg^{2+} ions allow these NMOFs to be unlocked. The "smart" carrier provides sense-and-treat functions

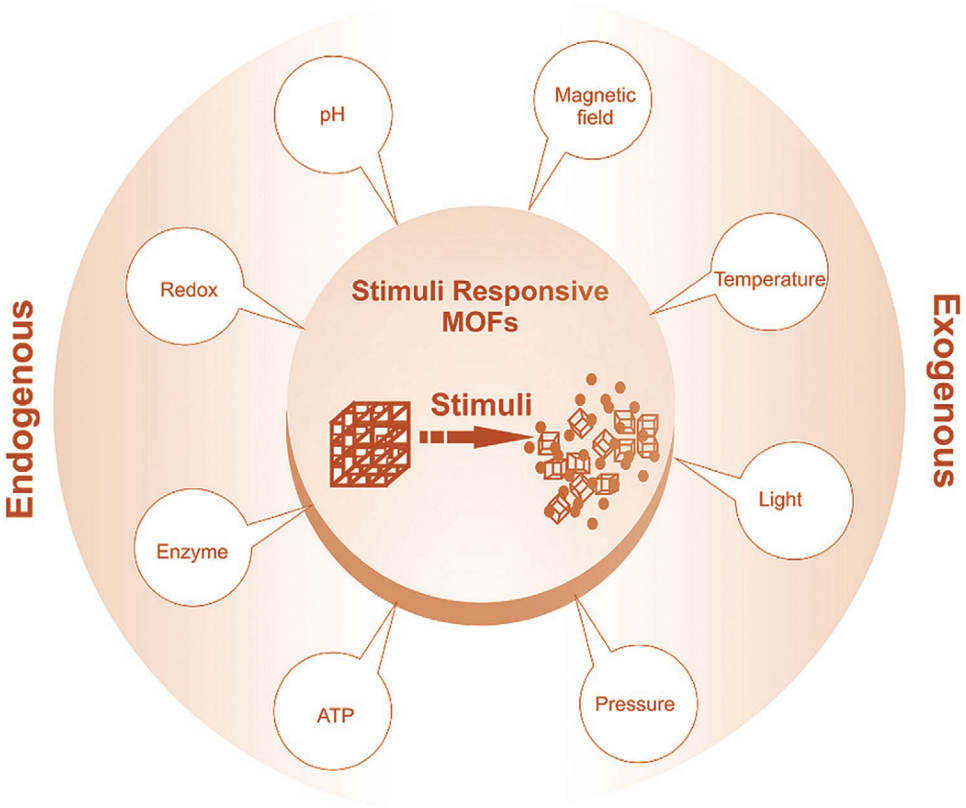

Figure 8. Schematic representation of different endogeneous and exogeneous stimuli-responsive based MOFs.

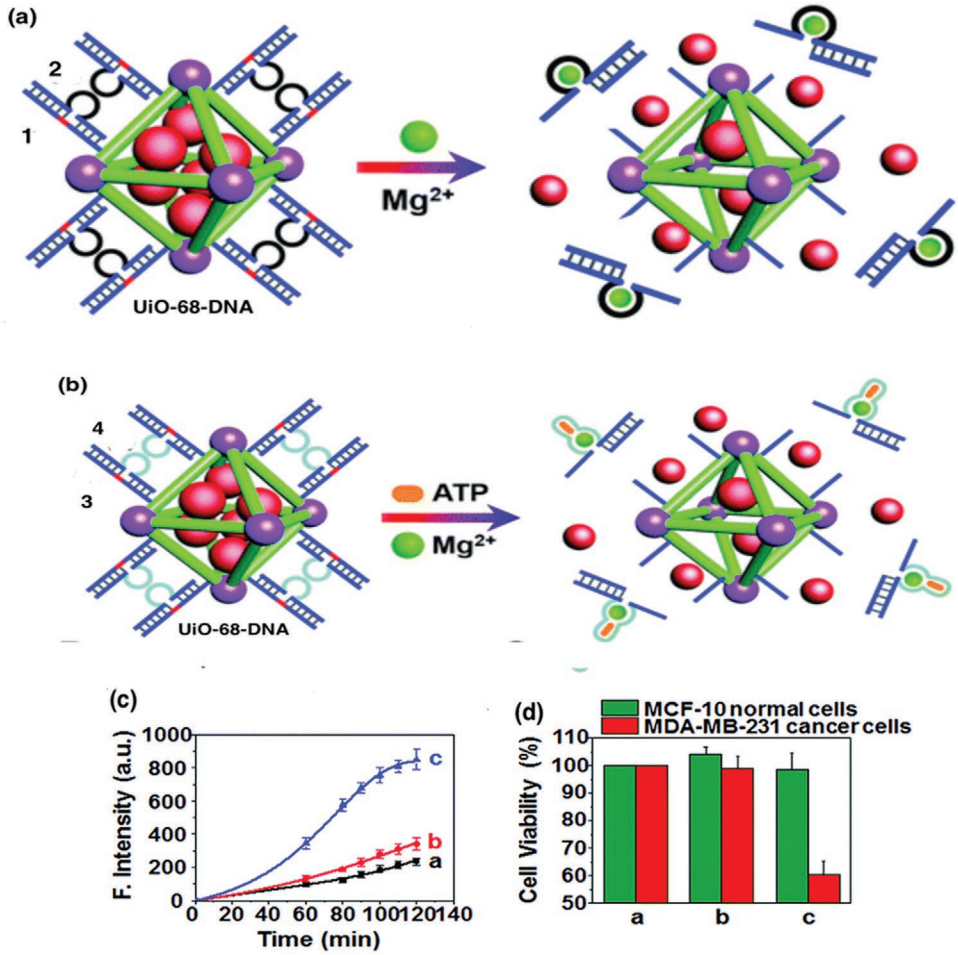

Figure 9. a) Mg^{2+}–ion-dependent DNAzyme-guided unlocking of loaded UiO-68 NMOFs. b) Cooperative ATP-driven activation of the Mg^{2+}-dependent DNAzyme units to unlock DOX-loaded UiO-68 MOFs. c) Time-dependent release of DOX from the (**3**)/(**4**)-locked drug-loaded UiO-68 NMOFs. d) Cytotoxicity of the (**3**)/(**4**)-locked DOX-loaded NMOFs toward MCF-10A normal epithelial breast cells and MDA-MB-231 breast cancer cells. Reproduced with permission.[48] Copyright 2017, Royal Society of Chemistry.

because ATP is overexpressed in cancer cells. The "smart" ATP/Mg^{2+}-triggered doxorubicin-loaded NMOFs also show preferential cytotoxicity toward MDA-MB-231 breast cancer cells and MCF-10A normal epithelial breast cells (**Figure 9**).

Recently, a redox dyshomeostasis (RDH) strategy is proposed by Bu's group, based on the pH/hypoxia/H_2O_2 triple stimuli–responsive nanoplatforms FeCysPW@ZIF-82@CAT Dz (Dz: DNAzymes, CAT: catalase) to disrupt redox homeostasis by enhancing intracellular H_2O_2 and decreasing glutathione (GSH) levels, as illustrated in **Figure 10**a. In an acidic environment, the ZIF-82@CAT Dz shell is degraded, releasing CAT Dz, free Zn^{2+} ions, and electrophilic ligands. The dissociated electrophilic ligands deplete GSH under hypoxic conditions, and the Zn^{2+} ions function as cofactors to accelerate CAT Dz-mediated CAT silencing to allow H_2O_2 buildup. RDH is produced in hypoxic cells by simultaneous increases in oxidants and antioxidants, resulting in increased intracellular H_2O_2, and chemodynamic therapy (CDT) has been employed to promote ROS-mediated apoptosis, which was also applied to enhance CDT-mediated hypoxic tumor therapy.[157] In the same year, Zhou and coworkers developed a metal–organic-framework-coated MnO_2 sheets that were rationally planned and created as nanocarriers for co-delivery of a survival blocking DNAzyme and DOX for chemogene combinatorial cancer therapy.[158] The assembly process for the probe is illustrated in Figure 10b. In this system, the MOF was coated under mild conditions concurrent with DNAzyme encapsulation, and the MnO_2 nanosheets were easily prepared to load DOX. In tumor cells, the nanosystem penetrates and degrades in response to intracellular stimuli, releasing DNAzyme and DOX. Thus, Mn^{2+} could operate as a metal cofactor for effective DNAzyme activation for survival downregulation to sensitize DOX-based cancer treatment, all while avoiding systemic toxicity. In the presence of abundant H_2O_2, in situ created Mn^{2+} activates the CDT by producing a highly toxic hydroxyl radical (·OH). This study provides an innovative technique to overcome the main limitations of DNAzymes for RNAi applications.

3.2. Applications of DNAzyme–AuNPs' Probes

Given the success of different preparation strategies for DNAzyme–gold nanoparticles, the most common applications of

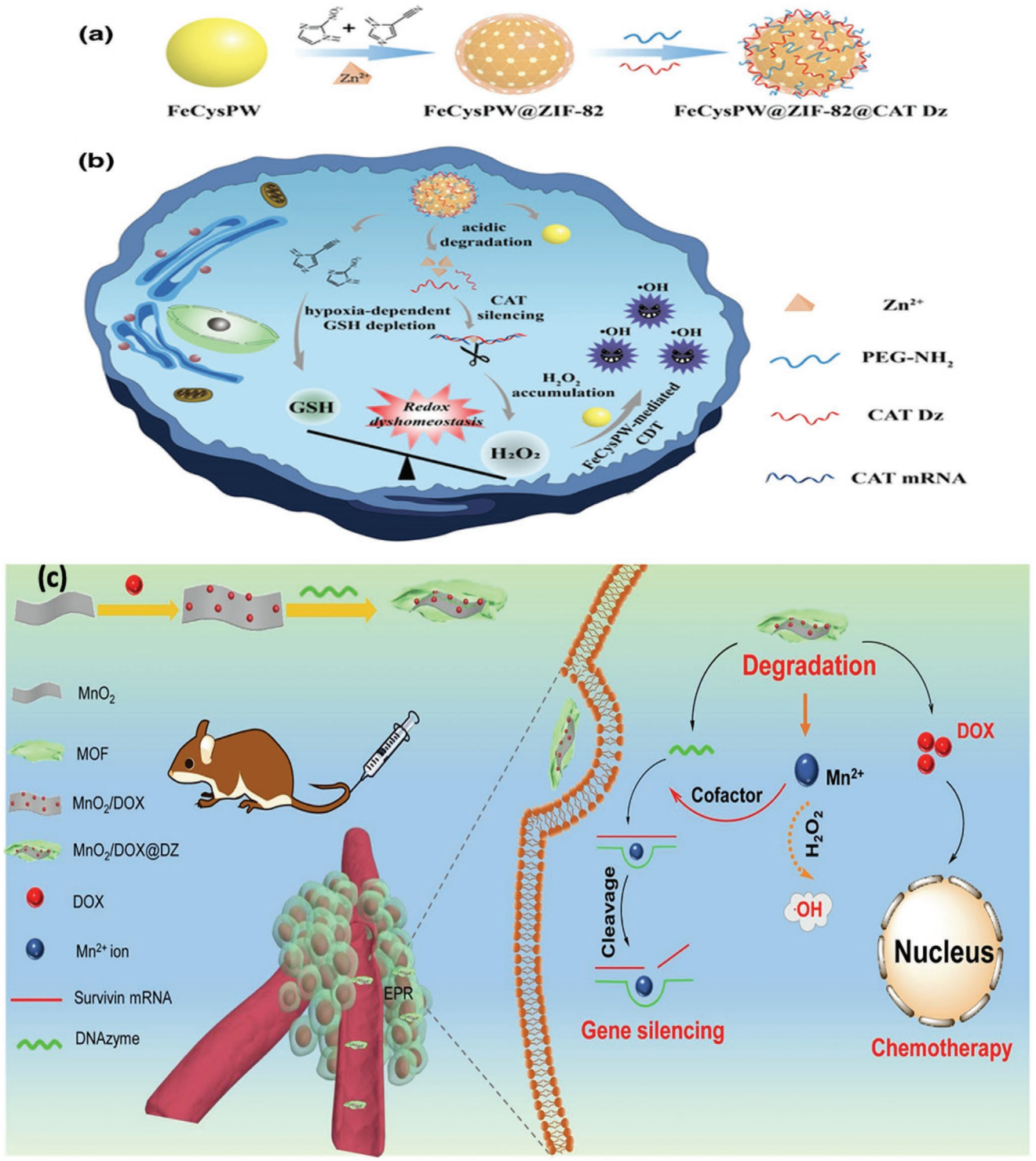

Figure 10. a,b) Schematic of the design and its applications of FeCysPW@ZIF-82@CAT Dz. Reproduced with permission.[157] Copyright 2020, Wiley-VCH. c) Schematic illustration of the construction of MnO_2/DOX@DNAzyme and its synergistic antitumor mechanism. Reproduced with permission.[158] Copyright 2020, Elsevier B.V.

these nanomaterials include i) biosensing; ii) bioimaging, which can accurately image metal ions and microRNAs; and iii) biomedical, which includes early disease diagnosis and drug delivery. The following sections introduce some of these properties.

3.2.1. DNAzyme–AuNPs as Biosensing and Imaging Platforms

AuNPs have a variety of useful signaling pathways, and DNAzyme can exploit their physical and chemical features for

sensing applications.[159,160] The surface chemistry of AuNPs, as well as their interactions with DNAzymes and targets, must be carefully considered when developing analytical biosensors. As mentioned above, in the signal output step, the sensors are classified into colorimetric sensors, electrochemical sensors, photo-electrochemical sensors, and other sensors (Table 1). Representative and recent examples of such biosensors are discussed in this section. AuNPs are optical materials with distance-dependent surface plasmon characteristics that cause significant color changes compared to those of organic dyes, making them suitable for colorimetric sensing. Using DNAzyme-directed assembly of AuNPs, Liu and Lu have developed highly selective Pb^{2+} biosensors with sensitivity tuning across several orders of magnitude.[161–164]

An early example that demonstrated DNAzyme-functionalized AuNPs to detect Pb^{2+} was developed by Liu and Lu in 2003.[165] That study first extended the substrate at each of the 3′and 5′ends as long as the recognition part of the enzyme is remained. At each end, the substrate strand (Sub_{Au}) was hybridized to the enzyme strand while retaining the 17E recognition portion. These hybridizations cause gold nanoparticle aggregation, which results in blue color. In the presence of Pb(II), however, the 17E catalyzes the hydrolytic cleavage of Sub_{Au}, preventing the formation of nanoparticle aggregates. As a result, a red color appears. This method yielded a limit of detection (LOD) of 100×10^{-9} M for Pb^{2+}. For other metal ions such as copper,[161,166] variations of the method using distinct DNAzymes have been developed. Interestingly, a sensitive and simultaneous approach for the detection of Pb^{2+} and Cu^{2+} was reported using a one-step strategy based on the pincer enzyme strand (E-DNA) and circular DNAzyme cleavage reaction.[167] The pincer E-DNA on the AuNPs can be labeled with the S-DNA to shape DNAzyme for simultaneous recognition of Pb^{2+} and Cu^{2+} ions. Furthermore, the fluorophore-labeled S-DNA was cleaved from the surface of the AuNPs with the aid of Pb^{2+} and Cu^{2+} as shown in **Figure 11**. After that, the pincer E-DNA was liberated for a circular catalytic cleavage reaction, which resulted in a considerable recovery of fluorescence intensities for both Pb^{2+} and Cu^{2+}. The LOD of 80×10^{-12} and 30×10^{-12} M for Pb^{2+} and Cu^{2+}, respectively, were attained with good sensitivity using an amplification technique. This method has great potential for detecting and imaging metal ions in environmental and biological systems at the same time.

For the intracellular imaging applications, Lu's group has published a variety of researches using DNAzymes in this field. The 39E enzyme strand, its substrate strand, and 13 nm AuNPs make up the DNAzyme–AuNPs' cellular sensor (39ES-AuNPs).[168] The enzyme strand was coated with a thiol group at the 3′ end for AuNP immobilization, while the substrate strand was functionalized with a Cy3 fluorophore at the 5′ end and BHQ-2 at the 3′ end as shown in **Figure 12**a. The fluorophore-labeled substrate strand is cleaved by the DNAzyme in the presence of uranyl, leading to the release of the shorter product chain carrying the Cy3 and enhanced fluorescence. Due to the difficulty in delivering the DNAzyme within cells, fluorescent probes with one-photon emission are not suitable. To address this constraint, Tang's group developed a fluorescent nanomaterial based on AuNPs–DNAzyme for simultaneous imaging of Zn^{2+} and Cu^{2+} in living systems.[169] This nanoprobe is highly selective, has good nuclease stability, and is biocompatible (Figure 12b).

By modifying a Zn^{2+}-specific DNAzyme (8-17ES), Zhang and co-workers reported a TP probe based on DNAzyme–AuNPs for imaging intracellular Zn^{2+} as shown in Figure 12c.[170] Instead of using UV light, Yang et al. designed conjugated photocaged DNAzymes onto lanthanide-doped upconversion nanoparticles (UCNPs) and successfully converted a deep tissue incorporating NIR from 980 to 365 nm emission. Zn^{2+} ions were imaged in cells using this system. Wang et al., on the other hand, designed a near-infrared photothermal method to deliver the DNAzymes into cells and undergo activation.[171] The hybridization of the system made up of a three-stranded DNAzyme precursor (TSDP) prevents the DNAzyme activity (Figure 12d). Increased temperature de-hybridized the TSDP to release the active DNAzyme, resulting in cleavage products bearing a fluorophore after the functionalization of the TSDP onto gold nanoparticles and under NIR light. This method was used to image Zn^{2+} in HeLa cells.

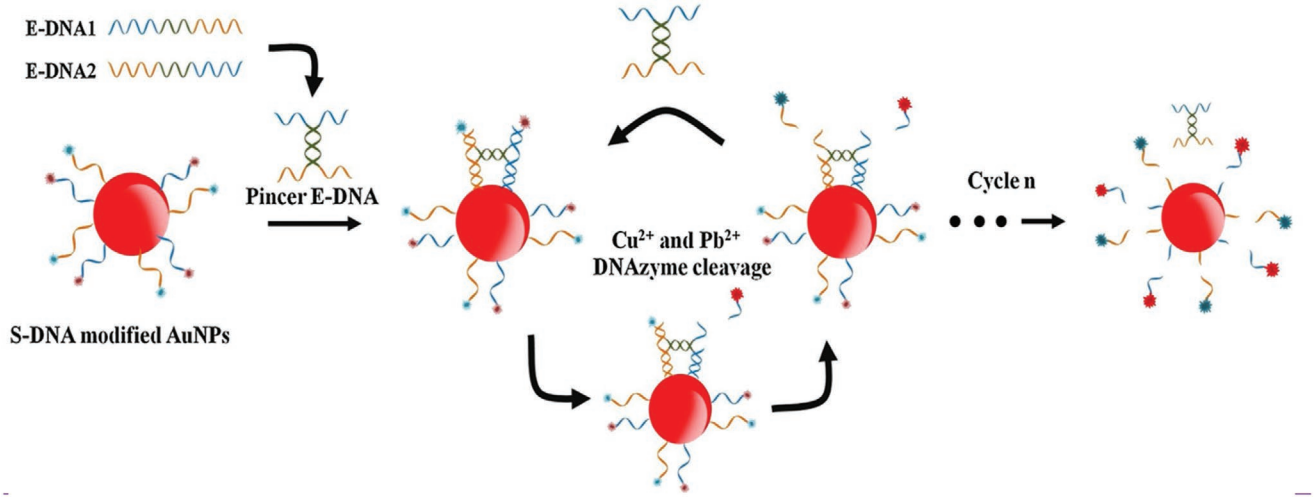

Figure 11. Schematic illustration of fluorescent nanoprobe for simultaneous determination of Pb^{2+} and Cu^{2+} based on E-DNA and signal amplification strategy. Reproduced with permission.[167] Copyright 2019, Elsevier B.V.

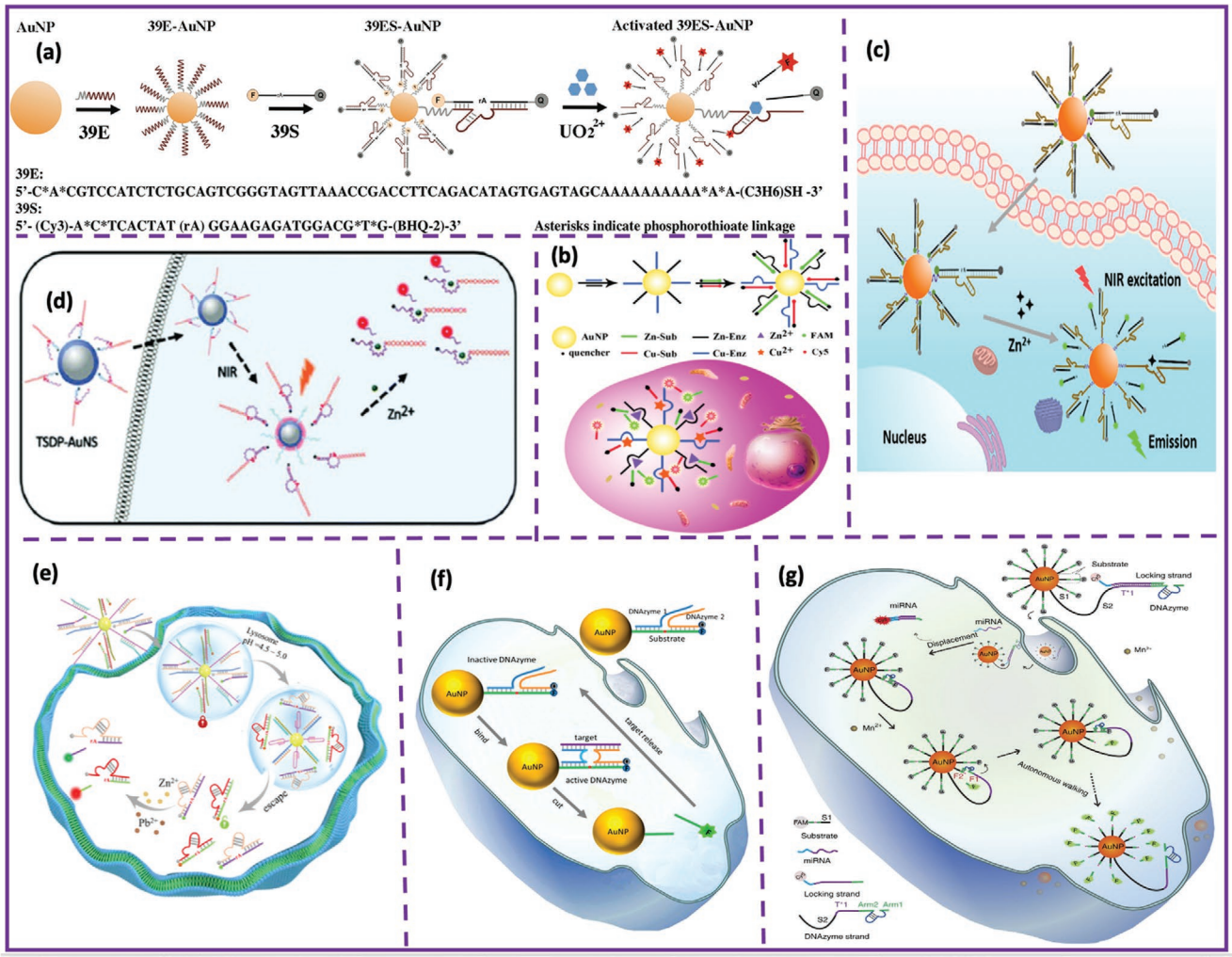

Figure 12. a) Illustration of fluorescent DNAzyme immobilized on AuNPs as the selective sensor of uranyl inside living cells. Reproduced with permission.[168] Copyright 2013, American Chemical Society. b) Simultaneous imaging of Zn^{2+} and Cu^{2+} in living cells based on DNAzyme-modified AuNPs. Reproduced with permission.[169] Copyright 2015, American Chemical Society. c) Design of a TP fluorescent DNAzyme conjugated AuNPs as a selective sensor of intracellular Zn^{2+}. Reproduced with permission.[170] Copyright 2018, American Chemical Society. d) Imaging of intracellular Zn^{2+} by the NIR photothermal activated DNAzyme–AuNPs. Reproduced with permission.[171] Copyright 2017, Royal Society of Chemistry. e) Acid-switchable DNAzyme nanodevice for imaging dual metal ions in the physiological environment. Reproduced with permission.[172] Copyright 2020, American Chemical Society. f) AuNPs loaded with split-DNAzyme probes for magnified detection. Reproduced with permission.[173] Copyright 2017, American Chemical Society. g) AuNPs–DNAzyme motor for amplified detection and bioimaging of the specific microRNA in living cells. Reproduced with permission.[174] Copyright 2017, Springer Nature.

Nevertheless, the traditional fluorescence probes are limited for their visual analysis of endogenous metal ions in living cells. To meet this challenge, Cui et al. developed an acid-switchable DNA (SW-DNA) immobilized on AuNPs.[172] When the nanodevice enters living cells, the SW-DNA changes its configuration from linear to a triplex under acidic cytoplasmic conditions (pH ≈ 4.5–5.0), and the hybridized strands are liberated. Then, they react with DNAzyme precursors to form the active DNAzyme, which can further realize multi-imaging of intracellular metal ions, Zn^{2+} and Pb^{2+} ions, as illustrated in Figure 12e. In addition to metal ions, Wu et al. developed a novel intracellular nanoprobe, employing AuNPs loaded with split DNAzyme to detect miRNAs under physiological microenvironment.[173] In their design, the target sequence could activate the DNAzyme, which can then continuously cleave the fluorophore-labeled substrate strands and result in fluorescence recovery. Two splits of DNAzymes construct an inactive DNA motif with its substrate in the absence of target miRNA using partial hybridization at the same time as the fluorescence is quenched. It also demonstrated excellent properties as an intracellular nanoprobe for cancer-related miRNA detection at physiological Mg^{2+} concentrations, with low cytotoxicity, great resistance to enzymatic degradation, and cellular permeability, resulting in a fluorescence signal that was amplified (Figure 12f). Interestingly, Peng et al. reported a DNAzyme motor that responds to a specific intracellular target in living cells.[174] This motor is made up of 20 nm AuNPs coated with substrate strands that serve as DNA tracks and DNAzyme structures that are individually muted by a locking strand as shown in Figure 12g. Intracellular-specific miRNA can hybridize with the locking strand, which causes the DNAzyme

motor to walk autonomously on the surface of the AuNPs. This AuNPs–DNAzyme motor was achieved magnified detection and bioimaging of the specific microRNAs in human cancer cells by exploiting a fuel-strand-triggered cleavage of substrate strands. Extra Mn^{2+} was added to increase DNAzyme activity. Since then, various intracellular miRNA detection designs based on DNA walkers or motor systems have been developed.[175–177]

3.2.2. DNAzyme@AuNPs' Platform for Enhanced Phototherapy

Nanoparticles have been widely studied as potential theranostic agents for cancer treatment in recent years. The capacity of AuNPs to resonantly absorb and scatter incident light (LSPR), causing solid localized surface plasmon resonance, makes them an attractive nanomaterial. Because of their high heat conversion efficiency and robust absorption, AuNPs can be employed for photothermal therapy. However, most PSs have limited water solubility, making delivery into cancer cells challenging. In this regard, using an excellent carrier could be a viable solution to the limitation of PDT for cancer therapy.[178,179] PSs can be delivered using AuNP–DNA conjugates. In 2017, Tang and co-workers designed gold nanomachines made from intelligent alpha-cyclodextrin (α-CD) for tumor-selective diagnosis and therapy.[178] The proposed α-CD caps prevent hybridization between DNA strands on gold nanoparticles, and resist clearance during blood circulation, have strong nuclease resistance, and helped preserve blood circulation stability.

However, in a mildly acidic tumor microenvironment, they are released, resulting in DNA hybridization and the formation of large-sized gold aggregates, capable of surviving in tumor regions despite high interstitial fluid pressure, as well as tumor-selective photoacoustic imaging and phototherapy for diagnosis and therapy, as shown in **Figure 13**a. Moreover, Long and co-workers introduced a binary system for miRNA-21 targeted imaging and photothermal treatment of single cells.[180] Both molecular beacon (MB)-conjugated AuNPs (MB-1/MB-2 for probe-1/probe-2, respectively, which are encapsulated in liposomes for cell delivery) consisted of this binary system. As shown in Figure 13b, the loop portion of the MB was designed to complement miRNA21. The absorption of AuNPs shifts to near-infrared as a result of miRNA-induced aggregation, which may be shown from DFM and exploited for photothermal therapy. Importantly, the suggested approach successfully eliminated MCF-7 breast cancer cells, and it has since been tested in tumor-bearing mice, demonstrating a considerable therapeutic impact with no obvious side effect effects (Figure 13b,c).

Recently, Kim and co-workers created a DNA–AuNPs dynamic nanomachine for combined antitumor therapy.[181] In their design,

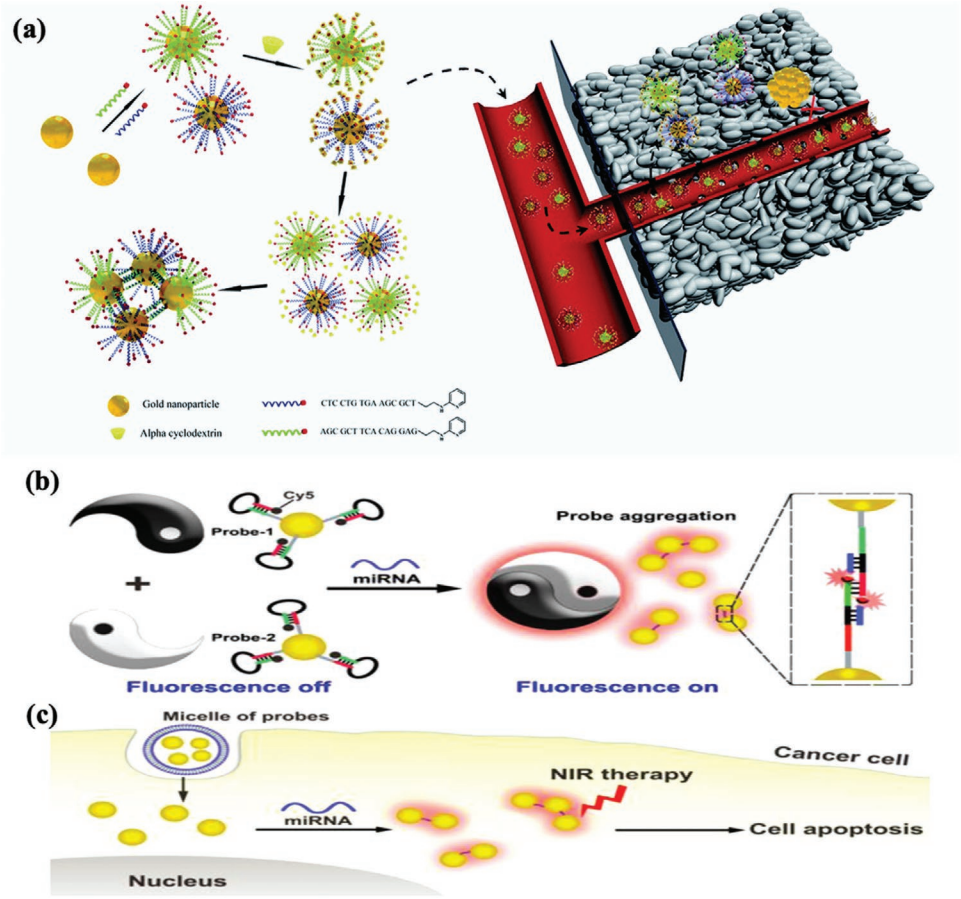

Figure 13. a) Mild-acid-triggered self-fabrication and tumor-specific photoacoustic imaging and photothermal therapy. Reproduced with permission.[178] Copyright 2017, Royal Society of Chemistry. b) A miRNA-21-induced gold nanoparticles and fluorescence "off–on". c) In situ imaging of miRNA-21 in MCF-7 cells and the miRNA-targeted NIR therapy. Reproduced with permission.[180] Copyright 2016, American Chemical Society.

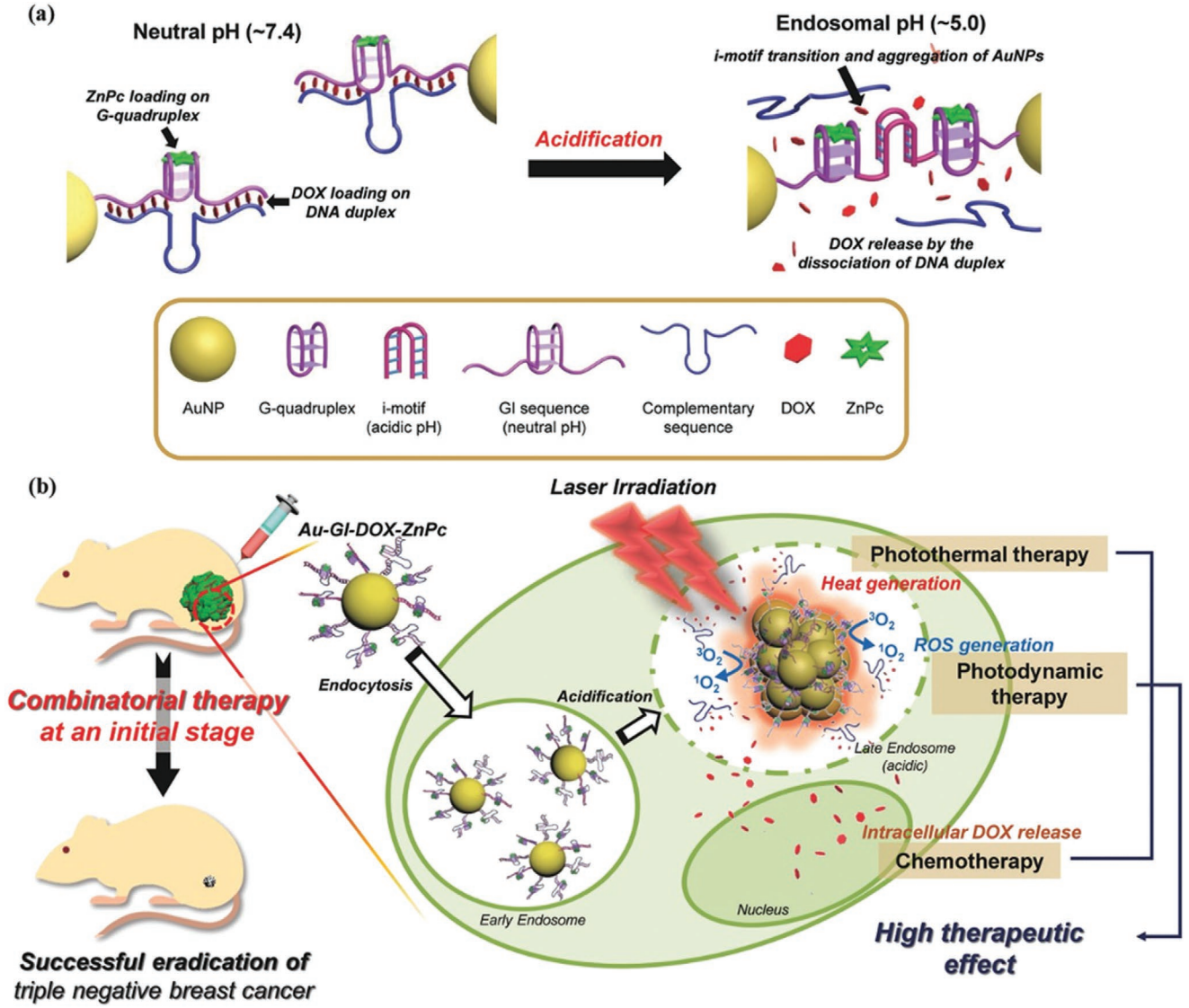

Figure 14. a) Design of the Au–GI nanomachine and its functional mechanism depending on pH. b) Intracellular dynamic operation of the Au–GI nanomachine inducing triple combinatorial anti-tumor therapy (chemo/photodynamic, and photothermal therapy. Adapted with permission.[181] Copyright 2017, John Wiley & Sons, Inc.

the surfaces of gold nanoparticles were modified with functional DNA containing the G-quadruplex and the i-motif sequence (GI). Furthermore, the i-motif hybridizes with its corresponding DNA sequence to produce a duplex DNA (cDNA). Then, with excellent selectivity, DOX and zinc phthalocyanine (ZnPc) were loaded inside the i-motif/cDNA duplex and G-quadruplex, respectively, as shown in **Figure 14**. This nanomachine showed intracellular pH-responsive dynamic activity and a synergistic therapeutic effect, resulting in triple chemo-/photodynamic and photothermal therapy.

3.2.3. Stimuli–Responsive Therapeutic Platform Based on DNAzyme@AuNPs

Another interesting application of DNAzyme-based nanostructures, the stimuli–responsive DNAzyme-conjugated gold nanoparticles, has emerged as an intelligent drug delivery system for cancer therapy. In recent years, there has been a resurgence in interest in using DNA–AuNPs' nanoplatforms to develop effective cancer therapy methods. However, the potential of the DNAzyme–AuNPs system as an intelligent drug carrier for stimuli–responsive in gene therapy has rarely been investigated. In this section, we discuss some representative examples of these therapeutic applications including exogenous stimuli and endogenous stimuli for DNAzyme-functionalized AuNPs.

In 2016, Zhu and co-workers proposed a GNPs-ES-DOX/ZnO nanomaterial that effectively delivered antisense miRNA and antitumor drugs for the combined gene modulation and drug release.[182] In this system, a Zn^{2+} ligation-dependent DNAzyme and AS1411 aptamer were made on gold nanoparticles through Au—S bonding, and by hybridization between the DNAzyme and its substrate strand as illustrated in **Figure 15**. Then, the

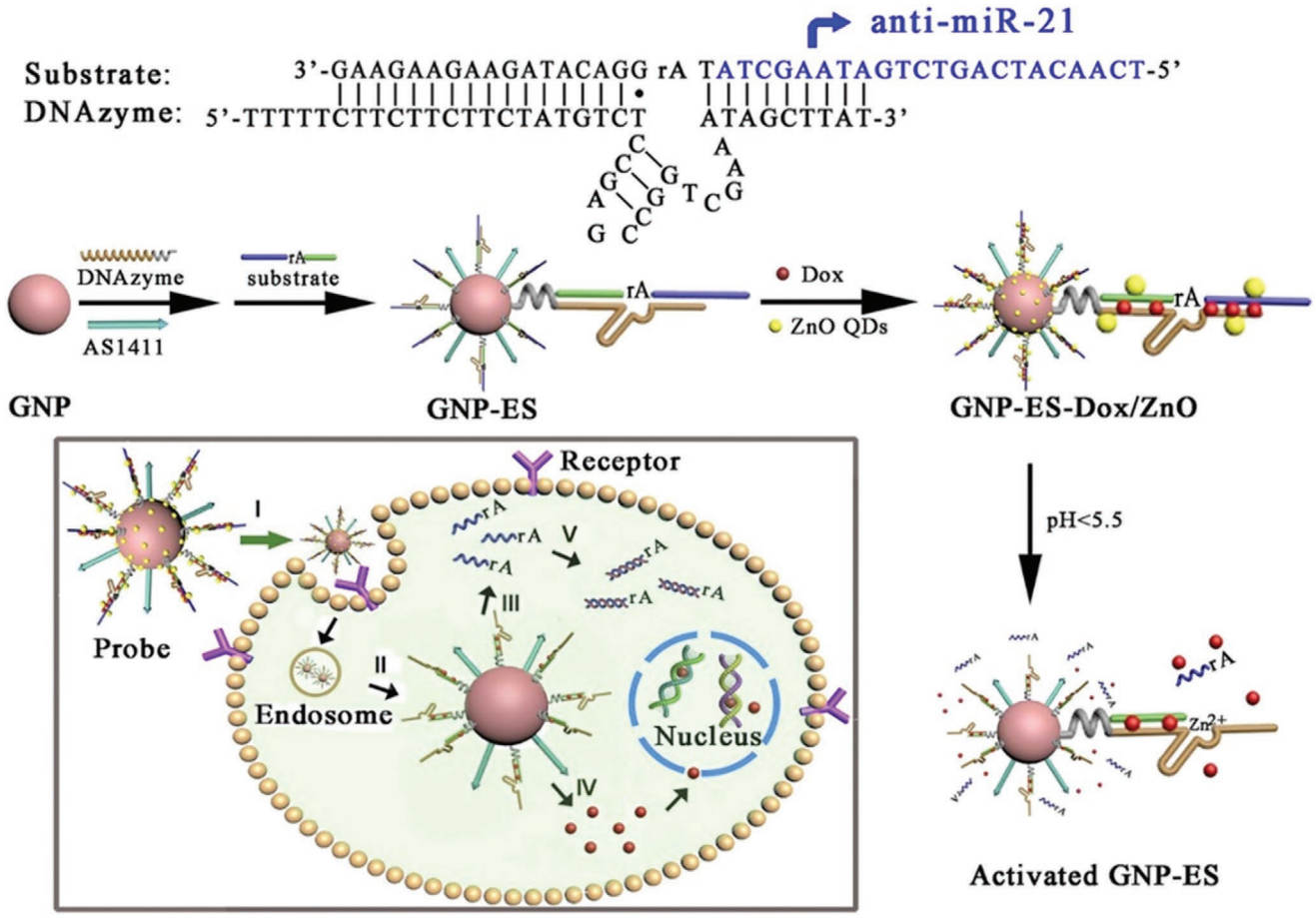

Figure 15. Schematic illustration of the nanoprobe GNPs-ES-DOX/ZnO for the combination of gene modulation and drug release. Reproduced with permission.[182] Copyright 2016, Springer Nature.

DOX was polymerized in the double-stranded GC pairs. Furthermore, positively charged ZnO@quantum dot (QDs) were electrostatically adsorbed onto the gold nanoparticles (GNPs) to assemble the intracellular probe (GNPs-ES-DOX/ZnO). Under an acidic environment, the release of DNAzyme is activated by Zn^{2+} ions, which are generated via the dissolution of ZnO@QDs. Such pH-sensitive nanocarriers have indicated that improved effective therapeutic efficacy can be achieved through the suppression of endogenous miR-21 levels, resulting in the inhibition of cell proliferation and activation of cell apoptosis.

3.3. DNAzyme–MoS_2 Nanoparticle Probes as Biosensing and Imaging Platforms

The combination of MoS_2 and DNAzyme recognition event outcomes in novel sensing platforms. However, biological applications of DNAzyme–MoS_2 nanosheets have only been developed once up until now. MoS_2 nanosheets can securely adsorb dye-loaded ssDNA and quench the dye fluorescence, but it has a lower affinity for dsDNA.[129]

Based on molybdenum disulfide nanosheets and DNAzymes, Fu and co-workers reported a turn-off fluorescence probe for the detection of uranyl ions.[130] UO_2^{2+}could cleave DNAzyme to release a 6-carboxylfluorescein (FAM)-labeled ssDNA in the presence UO_2^{2+}, and the liberated molecule can be effectively adsorbed to the surface of MoS_2 as illustrated in **Figure 16**. As a result, the fluorescence intensity was noticeably reduced. Moreover, MoS_2 nanosheets show a low affinity for the substrate–enzyme combination DNAzyme. With a recovery of 96–102% and an relative standard deviation (RSD) of <5% ($n = 6$), the suggested sensor was employed with an LOD of 2.14×10^{-9} M for UO_2^{2+} in an aqueous environment. As a result, a sensing platform with high sensitivity and stability, as well as swift analysis time, was developed for the detection of UO_2^{2+}.

3.4. DNAzyme–GO Nanoparticle Probes as Biosensing and Imaging Platforms

The combination of DNAzymes and GO frameworks has provided many possibilities for developing amplified fluorescence biosensors.

In 2011, Yu's group reported a GO–DNAzyme-based probe for Pb^{2+} "turn-on" detection via amplified fluorescence.[183] As shown in **Figure 17**, the substrate strand is tagged at the 5′ end with a FAM, which is hybridized to the DNAzyme strand to generate a DNAzyme–substrate hybrid with a wide ssDNA loop to interact with the GO. A FAM-labeled DNAzyme–substrate hybrid served

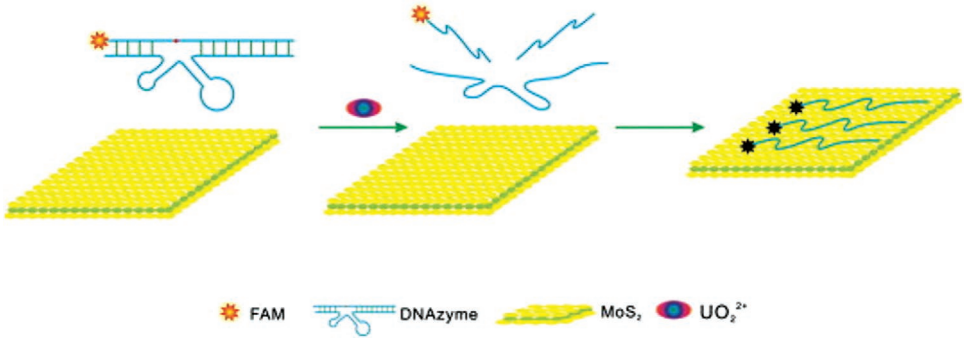

Figure 16. illustration of the detection principle of the suggested fluorescent biosensor DNAzyme–MoS_2. Reproduced with permission.[130] Copyright 2015, Elsevier B.V.

as a molecular recognition module as well as a signal reporter, while GO functioned as a super quencher. This sensing system was used to determine Pb^{2+} in an aqueous environment with an LOD of 300×10^{-12} M and had high sensitivity toward the target.

As mentioned in the following sections, Wen et al. presented a "turn-off" design in which the interactions between GO and an 8–17 DNAzyme revealed that Pb^{2+} may precisely modify the couplings by cleavage of the 17S substrate (**Figure 18**a). They used GO nanoprobe sensors with excellent sensitivity, selectivity, and programmable dynamics to extend a simple mix-and-detect fluorescence sensor for Pb^{2+} ions. Thus, the planar shape of graphene allows it to adsorb a variety of DNA probes.[132] In 2017, Huang's group designed a DNAzyme branched junction structure with three kinds of DNAzymes and GO for simultaneous fluorescent detection of Cu^{2+}, Pb^{2+}, and Mg^{2+}.[184] As illustrated in Figure 18b,c, three fluorophore-labeled DNA sequences containing E-DNA and S-DNA were fused to produce a DNAzyme binding structure. The S-DNA was cleaved and adsorbed on the GO surface under the target metal ion to quench the fluorescent signal. Furthermore, the detection limits for Cu^{2+}, Mg^{2+}, and Pb^{2+} were predicted to be 1×10^{-9}, 200×10^{-9}, and 0.3×10^{-9} M, respectively. This technique demonstrates how sensors can be used to detect and image numerous metal ions in environmental and biological systems.

Later, Radhakrishnan and co-workers reported on a fluorescent biosensing platform based on a self-assembled GO-DNAzyme complex for the detection of Pb(II) and Hg(II) ions.[185] The DNAzyme and substrate strands hybridize and attach to the surface of GO, which acts as a signal sensor while quenching the signal. When the Pb(II) ion enters the DNAzyme, it cleaves and releases fragments on the GO surface. The remarkable fluorescent intensity of the thioflavin T (ThT) fluorescent probe was due to its binding to the G-quadruplex, as shown in **Figure 19**. In addition, the detection limits of 96×10^{-12} M for Pb (II) and 356×10^{-12} M for Hg(II) were achieved within the range of 0 to 0.05×10^{-9} M. As a result, this suggested method has a high potential for detecting Pb(II) and Hg(II) ions in biological systems with excellent effects.

4. Summary and Future Outlook

Nanoparticles with distinct physical and chemical properties have trigged intensive interest in nanoscience fields. Especially,

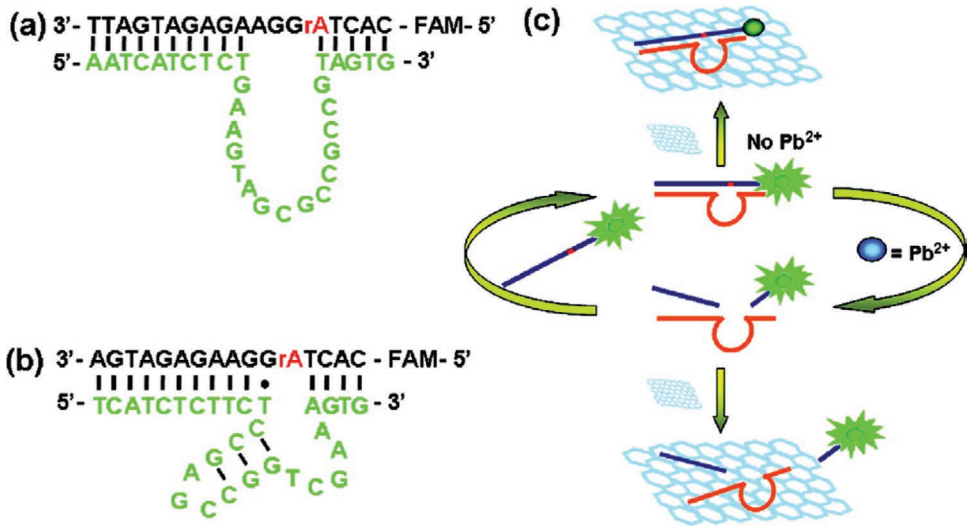

Figure 17. a) Illustration of secondary structure of the GR-5 DNAzyme hybridized with the FAM-labeled substrate strand. b) Secondary structure of the 8–17 DNAzyme hybridized with the FAM-labeled substrate strand; the "rA" adenosine ribonucleotide. c) Schematic illustration of the DNAzyme–GO based fluorescence sensor for Pb^{2+}. Reproduced with permission.[183] Copyright 2011, Elsevier B.V.

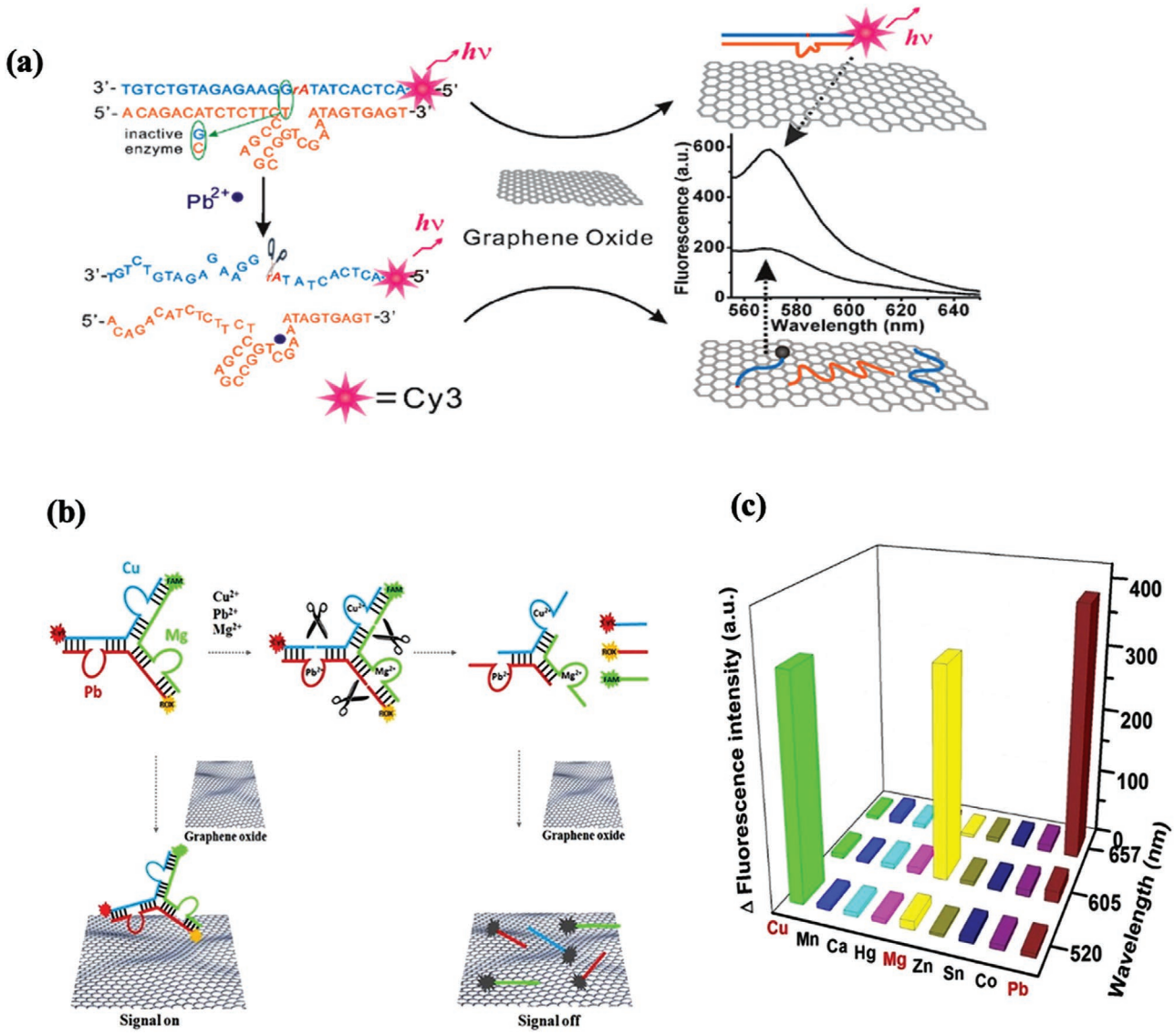

Figure 18. a) Schematic for the Pb^{2+}-modulated coordination between DNAzyme and GO. The fluorescence spectra of a mixture of DNAzyme and GO upon interaction with 0 to 2×10^{-3} M of Pb^{2+}. Reproduced with permission.[132] Copyright 2011, Royal Society of Chemistry. b) Illustration of the simultaneous fluorescent determination of Cu^{2+}, Pb^{2+}, and Mg^{2+} based on GO platform. c) The spectra of selectivity for the proposed biosensor. Reproduced with permission.[184] Copyright 2017, Elsevier B.V.

the development of inorganic and organic NPs with functional DNAzymes in living systems has attracted considerable attention and has emerged as a new area in biomedical research.

In this review, we summarized various methods for assembling DNAzymes with four surfaces types, including such as metal–organic frameworks, gold nanomaterials, graphene oxide, and molybdenum disulfide involving encapsulation, covalent conjugation, adsorption, and self-insertion. In addition, systematic studies regarding synthesis conditions, with the versatility in structure and function, were investigated in detail to better understand the interaction between these nanomaterials and DNAzyme. Meanwhile, with the advantages of optical, magnetic, and electronic properties and surfaces for immobilization offered by these nanosystems, we have highlighted the promising applications of DNAzyme–nanomaterial conjugates, particularly notable recent advances.

Overall, these nanoplatforms can be used to detect metals in aqueous solutions and can even be delivered into cells for bioimaging and biosensing. They can measure and image intracellular nucleic acids such as miRNA and mRNA. As reported, they can also serve as a carrier for phototherapy and stimuli–responsive drug delivery, which shows great promise in realizing the therapeutic effects. Given these signs of progress, there are still many challenges to overcome to further develop certain future directions in this emerging field along with the following aspects:

1) Several studies have shown that the use of DNAzyme–MOF conjugates for phototherapy has some drawbacks such as O_2-dependence, inhomogeneous heat distribution, and limited tissue delivery. This will necessitate the creation of more

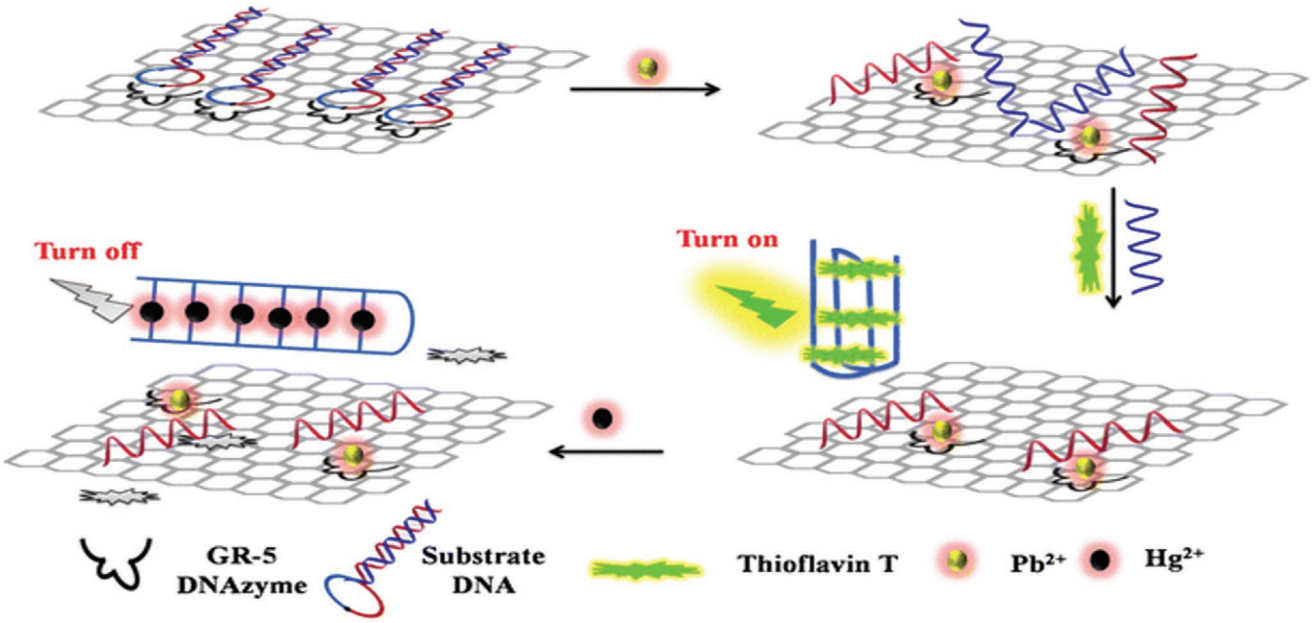

Figure 19. Illustration of the fluorescent detection of Pb(II) and Hg(II). Reproduced with permission.[168] Copyright 2018, Springer.

efficient synthetic routes to generate smaller MOFs with more homogeneous sizes, as well as the appropriate functionalization to improve stability in physiological media. With the advancements in the field of MOFs, it is believed that a precise understanding of the growth mechanisms of MOFs on the cell surfaces is crucial for the future development of DNAzyme@MOFs nanoplatforms for controlled biomedical applications. While several examples in the literature have employed covalent organic framework (COF) in fluorescence-based sensing platforms for DNA detection,[186–189] DNAzyme–COF complexes require further studies. This system will have greater selectivity, sensitivity, and stability, as well as a broader range of applications in chemistry, biology, and medicine.

2) The preparation of DNAzyme–AuNPs conjugated with specific DNAzyme strands and functionalization of diverse regions of AuNPs remains challenging. Numerous efforts are still to identify easy solutions to achieve these objectives. Moreover, the anchoring of DNAzyme on the surface of AuNPs via Au—S bonds is unstable in a variable environment. For breaking through this bottleneck, Yang's group and Tang's group developed a novel strategy via replacing the Au—S bond with Au—Se or Pt—S bond, respectively.[190,191] To ensure that the optimal DNAzyme activity has been driven primarily by controlling the interface between DNAzyme and nanomaterials. For instance, the density and orientation of DNAzymes are critical for the regulation of their activity.
3) Although many types of 2D nanomaterials interacting with DNA have been reported,[126,129,192–195] most of these studies have been performed on GO, MoS_2, and WS_2, which can all adsorb single-stranded DNA (**Table 2**). However, the interaction between GO and MoS_2 with DNAzyme has rarely been explored. These challenges will motivate researchers to develop new enhanced interaction methods and applications of DNAzymes with these kinds of nanomaterials. As a result, there is still much work to be done on developing diverse bonds between DNAzymes and nanomaterials for programming the construction of DNAzyme-functionalized nanomaterials for biomedical applications.
4) In terms of increasing the binding affinity of DNAzymes to metal ions, significant progress has been made. A large number of metal ions have been isolated from proteins and small molecules in cells. However, the free metals available for DNAzyme have rarely been discussed. Meanwhile, some new trends and challenges may be easily observed, such as the selection of various metal-ion-dependent DNAzymes and simulation of the binding mechanisms.[196,197]
5) It is also important that long-term subsequent monitoring of the organism is essential. Furthermore, current imaging studies and therapeutic applications are far from being used clinically, and a thorough understanding of the mechanism

Table 2. Typical examples of DNA–2D nanomaterial conjugates.

Nanomaterial	DNA probe	Ref.
TPA-COF	Single strand DNA	[188]
TpTta-COF	Single strand DNA and nucleotides	[189]
TTA–DFP COF	Single strand DNA	[187]
EB-TFB-COF	Label-free detection of double strand DNA	[186]
MoS_2	Single strand DNA	[126]
MoS_2	Double-stranded DNA	[129]
MoS_2-GO	Single strand DNA	[193]
WS_2	Single strand DNA	[192]
WS_2	Double-stranded DNA	[194]
TMDS (MoS_2, $MoSe_2$, WS_2, WSe_2)	Hairpin DNA	[195]

Ethidium bromide (EB); 2,6-diformylpyridine (DFP), 4,4′,4″-(1,3,5-triazine-2,4,6-triyl)trianiline (TTA); 1,3,5-triformylphloroglucinol (Tp), 4,4′,4″-(1,3,5-triazine-2,4,6-triyl)trianiline (Tta); transition metal dichalcogenides (TMDs).

of absorption, metabolism, and excretion is required. Finally, future efforts should focus on increasing the binding affinity of DNAzymes to metal ions, in combination with various mechanisms to achieve excellent efficacy in cancer or other diseases. Although DNAzyme-based nanotherapeutic platforms for clinical applications remain a long-standing challenge in nanomedical development, groups of researchers have made significant progress. Therefore, more attention could be paid to the development of the new DNAzyme/nanomaterials conjugates to address these challenges.

Acknowledgements

This work was supported by the Science and Technology Innovation Commission of Shenzhen, China (Grant No. KQJSCX20180328095517269) and Top Young Talent of the Pearl River Talent Recruitment Program, China.

Conflict of Interest

The authors declare no conflict of interest.

Keywords

biosensing, DNAzymes, MOFs/AuNPs/GO/MoS_2, nanomaterials, stimuli–responsive nanoplatforms

Received: September 7, 2021
Revised: October 14, 2021
Published online: November 21, 2021

[1] M. Rothenbroker, E. M. McConnell, J. Gu, M. L. Urbanus, S. E. Samani, A. W. Ensminger, C. D. M. Filipe, Y. Li, *Angew. Chem., Int. Ed.* **2021**, *60*, 4782.
[2] I. Cozma, E. M. McConnell, J. D. Brennan, Y. Li, *Biosens. Bioelectron.* **2021**, *177*, 112972.
[3] S. E. Samani, D. Chang, E. M. McConnell, M. Rothenbroker, C. D. M. Filipe, Y. Li, *ChemBioChem* **2020**, *21*, 632.
[4] L. Ma, J. Liu, *iScience* **2020**, *23*, 100815.
[5] M. Liu, D. Chang, Y. Li, *Acc. Chem. Res.* **2017**, *50*, 2273.
[6] R. R. Beaker, G. F. Joyce, *Chem. Biol.* **1994**, *1*, 223.
[7] D. Baum, S. Silverman, *Cell. Mol. Life Sci.* **2008**, *65*, 2156.
[8] S. W. Santoro, G. F. Joyce, *Biochemistry* **1998**, *37*, 13330.
[9] G. A. Soukup, R. R. Breaker, *RNA* **1999**, *5*, 1308.
[10] S. W. Santoro, G. F. Joyce, *Proc. Natl. Acad. Sci. USA* **1997**, *94*, 4262.
[11] Z. Xu, L. Yang, L. Sun, Y. Cao, *Chin. Sci. Bull.* **2012**, *57*, 3404.
[12] T. Cao, Y. Wang, Y. Tao, L. Zhang, Y.-L. Zhou, X.-X. Zhang, J. A. Heyman, D. A. Weitz, *Chem. Commun.* **2020**, *56*, 647.
[13] T. Lan, K. Furuya, Y. Lu, *Chem. Commun.* **2010**, *46*, 3896.
[14] J. Liu, Y. Lu, *J. Am. Chem. Soc.* **2007**, *129*, 9838.
[15] W. Zhou, R. Saran, Q. Chen, J. Ding, J. Liu **2016**.
[16] S.-F. Torabi, P. Wu, C. E. McGhee, L. Chen, K. Hwang, N. Zheng, J. Cheng, Y. Lu, *Proc. Natl. Acad. Sci. USA* **2015**, *112*, 5903.
[17] P. Travascio, Y. Li, D. Sen, *Chem. Biol.* **1998**, *5*, 505.
[18] G. Pelossof, R. Tel-Vered, J. Elbaz, I. Willner, *Anal. Chem.* **2010**, *82*, 4396.
[19] E. Golub, H. B. Albada, W.-C. Liao, Y. Biniuri, I. Willner, *J. Am. Chem. Soc.* **2016**, *138*, 164.
[20] R. J. Lake, Z. Yang, J. Zhang, Y. Lu, *Acc. Chem. Res.* **2019**, *52*, 3275.
[21] J. Huang, X. Su, Z. Li, *Biosens. Bioelectron.* **2017**, *96*, 127.
[22] D. Morrison, M. Rothenbroker, Y. Li, *Small Methods* **2018**, *2*, 1700319.
[23] I. Cozma, E. M. McConnell, J. D. Brennan, Y. Li, *Biosens. Bioelectron.* **2021**, *177*, 112972.
[24] W. Huo, X. Li, B. Wang, H. Zhang, J. Zhang, X. Yang, Y. Jin, *Biophys. Rep.* **2020**, *6*, 256.
[25] R. Freund, O. Zaremba, G. Arnauts, R. Ameloot, G. Skorupskii, M. Dincă, A. Bavykina, J. Gascon, A. Ejsmont, J. Gościańska, *Angew. Chem., Int. Ed.* **2021**, *60*, 23975.
[26] W. H. Chen, M. Vazquez-Gonzalez, A. Zoabi, R. Abu-Reziq, I. Willner, *Nat. Catal.* **2018**, *1*, 689.
[27] M. T. Zhao, K. Yuan, Y. Wang, G. D. Li, J. Guo, L. Gu, W. P. Hu, H. J. Zhao, Z. Y. Tang, *Nature* **2016**, *539*, 76.
[28] V. Stavila, R. Parthasarathi, R. W. Davi, F. El Gabaly, K. L. Sale, B. A. Simmons, S. Singh, M. D. Allendorf, *ACS Catal.* **2016**, *6*, 55.
[29] J. W. Liu, L. F. Chen, H. Cui, J. Y. Zhang, L. Zhang, C. Y. Su, *Chem. Soc. Rev.* **2014**, *43*, 6011.
[30] M. Yoon, R. Srirambalaji, K. Kim, *Chem. Rev.* **2012**, *112*, 1196.
[31] J. A. Hurd, R. Vaidhyanathan, V. Thangadurai, C. I. Ratcliffe, I. L. Moudrakovski, G. K. H. Shimizu, *Nat. Chem.* **2009**, *1*, 705.
[32] A. Shigematsu, T. Yamada, H. Kitagawa, *J. Am. Chem. Soc.* **2011**, *133*, 2034.
[33] J. Guo, Y. Zhang, Y. Zhu, C. Long, M. Zhao, M. He, X. Zhang, J. Lv, B. Han, Z. Tang, *Angew. Chem., Int. Ed.* **2018**, *57*, 6873.
[34] Y. Li, R. T. Yang, *Langmuir* **2007**, *23*, 12937.
[35] N. L. Rosi, J. Eckert, M. Eddaoudi, D. T. Vodak, J. Kim, M. O'Keeffe, O. M. Yaghi, *Science* **2003**, *300*, 1127.
[36] S. J. Yang, T. Kim, J. H. Im, Y. S. Kim, K. Lee, H. Jung, C. R. Park, *Chem. Mater.* **2012**, *24*, 464.
[37] S. Dang, E. Ma, Z. M. Sun, H. J. Zhang, *J. Mater. Chem.* **2012**, *22*, 16920.
[38] L. E. Kreno, K. Leong, O. K. Farha, M. Allendorf, R. P. Van Duyne, J. T. Hupp, *Chem. Rev.* **2012**, *112*, 1105.
[39] L. L. Wu, Z. Wang, S. N. Zhao, X. Meng, X. Z. Song, J. Feng, S. Y. Song, H. J. Zhang, *Chem. - Eur. J.* **2016**, *22*, 477.
[40] M. Zheng, H. Q. Tan, Z. G. Xie, L. G. Zhang, X. B. Jing, Z. C. Sun, *ACS Appl. Mater. Interfaces* **2013**, *5*, 1078.
[41] S. Zhang, X. Pei, H. Gao, S. Chen, J. Wang, *Chin. Chem. Lett.* **2020**, *31*, 1060.
[42] Y. T. Li, J. Jin, D. W. Wang, J. W. Lv, K. Hou, Y. L. Liu, C. Y. Chen, Z. Y. Tang, *Nano Res.* **2018**, *11*, 3294.
[43] W. Morris, W. E. Briley, E. Auyeung, M. D. Cabezas, C. A. Mirkin, *J. Am. Chem. Soc.* **2014**, *136*, 7261.
[44] C. B. He, K. D. Lu, D. M. Liu, W. B. Lin, *J. Am. Chem. Soc.* **2014**, *136*, 5181.
[45] J. T. Yi, T. T. Chen, J. Huo, X. Chu, *Anal. Chem.* **2017**, *89*, 12351.
[46] Y. Zhang, F. M. Wang, E. G. Ju, Z. Liu, Z. W. Chen, J. S. Ren, X. G. Qu, *Adv. Funct. Mater.* **2016**, *26*, 6454.
[47] S. Peng, B. L. Bie, Y. Z. S. Sun, M. Liu, H. J. Cong, W. T. Zhou, Y. C. Xia, H. Tang, H. X. Deng, X. Zhou, *Nat. Commun.* **2018**, *9*, 1293.
[48] W. H. Chen, X. Yu, A. Cecconello, Y. S. Sohn, R. Nechushtai, I. Willner, *Chem. Sci.* **2017**, *8*, 5769.
[49] J. S. Kahn, L. Freage, N. Enkin, M. A. A. Garcia, I. Willner, *Adv. Mater.* **2017**, *29*, 1602782.
[50] T. M. McDonald, J. A. Mason, X. Q. Kong, E. D. Bloch, D. Gygi, A. Dani, V. Crocella, F. Giordanino, S. O. Odoh, W. S. Drisdell, B. Vlaisavljevich, A. L. Dzubak, R. Poloni, S. K. Schnell, N. Planas, K. Lee, T. Pascal, L. W. F. Wan, D. Prendergast, J. B. Neaton, B. Smit, J. B. Kortright, L. Gagliardi, S. Bordiga, J. A. Reimer, J. R. Long, *Nature* **2015**, *519*, 303.
[51] K. Liang, J. J. Richardson, C. J. Doonan, X. Mulet, Y. Ju, J. W. Cui, F. Caruso, P. Falcaro, *Angew. Chem., Int. Ed.* **2017**, *56*, 8510.

[52] H. Yin, K. J. Kauffman, D. G. Anderson, *Nat. Rev. Drug Discovery* **2017**, *16*, 387.
[53] L. Vigderman, B. P. Khanal, E. R. Zubarev, *Adv. Mater.* **2012**, *24*, 4811.
[54] R. Elghanian, J. J. Storhoff, R. C. Mucic, R. L. Letsinger, C. A. Mirkin, *Science* **1997**, *277*, 1078.
[55] Z. L. Mao, R. Espinoza, A. Garcia, A. Enwright, H. Vang, S. C. Nguyen, *ACS Nano* **2020**, *14*, 7038.
[56] K. Saha, S. S. Agasti, C. Kim, X. N. Li, V. M. Rotello, *Chem. Rev.* **2012**, *112*, 2739.
[57] R. A. Sperling, P. Rivera gil, F. Zhang, M. Zanella, W. J. Parak, *Chem. Soc. Rev.* **2008**, *37*, 1896.
[58] M. Bouche, J. C. Hsu, Y. C. Dong, J. Kim, K. Taing, D. P. Cormode, *Bioconjugate Chem.* **2020**, *31*, 303.
[59] M. Sharifi, F. Attar, A. A. Saboury, K. Akhtari, N. Hooshmand, A. Hasan, M. A. El-Sayed, M. Falahati, *J. Controlled Release* **2019**, *311*, 170.
[60] S. Saha, X. H. Xiong, P. K. Chakraborty, K. Shameer, R. R. Arvizo, R. A. Kudgus, S. K. D. Dwivedi, M. N. Hossen, E. M. Gillies, J. D. Robertson, J. T. Dudley, R. A. Urrutia, R. G. Postier, R. Bhattacharya, P. Mukherjee, *ACS Nano* **2016**, *10*, 10636.
[61] W. Zhou, X. Gao, D. B. Liu, X. Y. Chen, *Chem. Rev.* **2015**, *115*, 10575.
[62] H. Kang, J. T. Buchman, R. S. Rodriguez, H. L. Ring, J. Y. He, K. C. Bantz, C. L. Haynes, *Chem. Rev.* **2019**, *119*, 664.
[63] C. Parolo, A. de la Escosura-Muniz, A. Merkoci, *Biosens. Bioelectron.* **2013**, *40*, 412.
[64] K. A. Mahmoud, K. B. Male, S. Hrapovic, J. H. T. Luong, *ACS Appl. Mater. Interfaces* **2009**, *1*, 1383.
[65] A. Sharma, Z. Matharu, G. Sumana, P. R. Solanki, C. G. Kim, B. D. Malhotra, *Thin Solid Films* **2010**, *519*, 1213.
[66] G. K. Ahirwal, C. K. Mitra, *Biosens. Bioelectron.* **2010**, *25*, 2016.
[67] J. H. Choi, H. S. Kim, J. W. Choi, J. W. Hong, Y. K. Kim, B. K. Oh, *Biosens. Bioelectron.* **2013**, *49*, 415.
[68] S. Gupta, H. Andresen, J. E. Ghadiali, M. M. Stevens, *Small* **2010**, *6*, 1509.
[69] M. X. Yu, J. Xu, J. Zheng, *Angew. Chem., Int. Ed.* **2019**, *58*, 4112.
[70] Y. F. Hu, Z. C. Huang, B. W. Liu, J. W. Liu, *ACS Appl. Nano Mater.* **2021**, *4*, 1377.
[71] B. Chen, L. Mei, R. R. Fan, Y. L. Wang, C. L. Nie, A. P. Tong, G. Guo, *Chin. Chem. Lett.* **2021**, *32*, 1775.
[72] L. Li, H. Xing, J. Zhang, Y. Lu, *Acc. Chem. Res.* **2019**, *52*, 2415.
[73] J. F. Chang, X. Wang, J. Wang, H. Y. Li, F. Li, *Anal. Chem.* **2019**, *91*, 3604.
[74] Z. R. Goddard, M. J. Marin, D. A. Russell, M. Searcey, *Chem. Soc. Rev.* **2020**, *49*, 8774.
[75] J. Azadmanjiri, P. Kumar, V. K. Srivastava, Z. Sofer, *ACS Appl. Nano Mater.* **2020**, *3*, 3116.
[76] X. Gan, H. Zhao, R. Schirhagl, X. Quan, *Mikrochim. Acta* **2018**, *185*, 478.
[77] Z. B. Li, S. L. Wong, *Mater. Sci. Eng., C* **2017**, *70*, 1095.
[78] B. W. Liu, S. Salgado, V. Maheshwari, J. W. Liu, *Curr. Opin. Colloid Interface Sci.* **2016**, *26*, 41.
[79] Y. Zhang, B. Zheng, C. Zhu, X. Zhang, C. Tan, H. Li, B. Chen, J. Yang, J. Chen, Y. Huang, L. Wang, H. Zhang, *Adv. Mater.* **2015**, *27*, 935.
[80] J. H. Huang, L. Ye, X. Gao, H. Li, J. B. Xu, Z. G. Li, *J. Mater. Chem. B* **2015**, *3*, 2395.
[81] Z. B. Liu, B. W. Liu, J. S. Ding, J. W. Liu, *Anal. Bioanal. Chem.* **2014**, *406*, 6885.
[82] R. M. Kong, L. Ding, Z. J. Wang, J. M. You, F. L. Qu, *Anal. Bioanal. Chem.* **2015**, *407*, 369.
[83] J. Ge, E. C. Ou, R. Q. Yu, X. Chu, *J. Mater. Chem. B* **2014**, *2*, 625.
[84] M. Zandieh, J. Liu, *Langmuir* **2020**, *36*, 3260.
[85] Z. Hu, Z. Suo, W. Liu, B. Zhao, F. Xing, Y. Zhang, L. Feng, *Biosens. Bioelectron.* **2019**, *131*, 237.
[86] B. W. Liu, L. Z. Ma, Z. C. Huang, H. Hu, P. Wu, J. W. Liu, *Mater. Horiz.* **2018**, *5*, 65.
[87] R. H. Yang, J. Y. Jin, Y. Chen, N. Shao, H. Z. Kang, Z. Xiao, Z. W. Tang, Y. R. Wu, Z. Zhu, W. H. Tan, *J. Am. Chem. Soc.* **2008**, *130*, 8351.
[88] W. J. Moon, J. Liu, *Adv. Mater. Interfaces* **2020**, *7*, 2001017.
[89] W. Xu, W. He, Z. Du, L. Zhu, K. Huang, Y. Lu, Y. Luo, *Angew. Chem., Int. Ed.* **2021**, *60*, 6890.
[90] W. J. Moon, Y. Yang, J. Liu, *ChemBioChem* **2021**, *22*, 779.
[91] L. Hu, X. Fu, G. Kong, Y. Yin, H. M. Meng, G. Ke, X. B. Zhang, *J. Mater. Chem. B* **2020**, *8*, 9449.
[92] J. Zhang, T. Lan, Y. Lu, *Adv. Healthcare Mater.* **2019**, *8*, 1801158.
[93] Y. Li, K. Zhang, P. Liu, M. Chen, Y. Zhong, Q. Ye, M. Q. Wei, H. Zhao, Z. Tang, *Adv. Mater.* **2019**, *31*, 1901570.
[94] A. Poddar, J. J. Conesa, K. Liang, S. Dhakal, P. Reineck, G. Bryant, E. Pereiro, R. Ricco, H. Amenitsch, C. Doonan, X. Mulet, C. M. Doherty, P. Falcaro, R. Shukla, *Small* **2019**, *15*, 1902268.
[95] H. M. Wang, Y. Q. Chen, H. Wang, X. Q. Liu, X. Zhou, F. Wang, *Angew. Chem., Int. Ed.* **2019**, *58*, 7380.
[96] S. Z. Wang, Y. J. Chen, S. Y. Wang, P. Li, C. A. Mirkin, O. K. Farha, *J. Am. Chem. Soc.* **2019**, *141*, 2215.
[97] T. M. Herne, M. J. Tarlov, *J. Am. Chem. Soc.* **1997**, *119*, 8916.
[98] J. C. Love, L. A. Estroff, J. K. Kriebel, R. G. Nuzzo, G. M. Whitesides, *Chem. Rev.* **2005**, *105*, 1103.
[99] J. Liu, Y. Lu, *Nat. Protoc.* **2006**, *1*, 246.
[100] B. Liu, J. W. Liu, *Anal. Methods* **2017**, *9*, 2633.
[101] W. H. Zhou, F. Wang, J. S. Ding, J. W. Liu, *ACS Appl. Mater. Interfaces* **2014**, *6*, 14795.
[102] C. A. Mirkin, R. L. Letsinger, R. C. Mucic, J. J. Storhoff, *Nature* **1996**, *382*, 607.
[103] J. I. Cutler, E. Auyeung, C. A. Mirkin, *J. Am. Chem. Soc.* **2012**, *134*, 1376.
[104] F. Schulz, T. Vossmeyer, N. G. Bastus, H. Weller, *Langmuir* **2013**, *29*, 9897.
[105] H. Pei, F. Li, Y. Wan, M. Wei, H. J. Liu, Y. Su, N. Chen, Q. Huang, C. H. Fan, *J. Am. Chem. Soc.* **2012**, *134*, 11876.
[106] F. Li, H. Pei, L. H. Wang, J. X. Lu, J. M. Gao, B. W. Jiang, X. C. Zhao, C. H. Fan, *Adv. Funct. Mater.* **2013**, *23*, 4140.
[107] Z. D. Wang, J. Q. Zhang, J. M. Ekman, P. J. A. Kenis, Y. Lu, *Nano Lett.* **2010**, *10*, 1886.
[108] J. W. Liu, *Phys. Chem. Chem. Phys.* **2012**, *14*, 10485.
[109] B. W. Liu, P. Wu, Z. C. Huang, L. Z. Ma, J. W. Liu, *J. Am. Chem. Soc.* **2018**, *140*, 4499.
[110] L. K. Wolf, Y. Gao, R. M. Georgiadis, *Langmuir* **2004**, *20*, 3357.
[111] H. Kimura-Suda, D. Y. Petrovykh, M. J. Tarlov, L. J. Whitman, *J. Am. Chem. Soc.* **2003**, *125*, 9014.
[112] G. B. Yao, J. Li, Q. Li, X. L. Chen, X. G. Liu, F. Wang, Z. B. Qu, Z. L. Ge, R. P. Narayanan, D. Williams, H. Pei, X. L. Zuo, L. H. Wang, H. Yan, B. Feringa, C. H. Fan, *Nat. Mater.* **2020**, *19*, 781.
[113] G. B. Yao, H. Pei, J. Li, Y. Zhao, D. Zhu, Y. N. Zhang, Y. F. Lin, Q. Huang, C. H. Fan, *NPG Asia Mater.* **2015**, *7*, e159.
[114] X. Zhang, M. R. Servos, J. W. Liu, *J. Am. Chem. Soc.* **2012**, *134*, 7266.
[115] B. W. Liu, J. W. Liu, *J. Am. Chem. Soc.* **2017**, *139*, 9471.
[116] B. W. Liu, T. Y. Wu, Z. C. Huang, Y. B. Liu, J. W. Liu, *Angew. Chem., Int. Ed.* **2019**, *58*, 2109.
[117] Z. C. Huang, B. W. Liu, J. W. Liu, *Langmuir* **2016**, *32*, 11986.
[118] B. W. Liu, J. W. Liu, *Langmuir* **2019**, *35*, 6476.
[119] K. J. Huang, Y. J. Liu, H. B. Wang, Y. Y. Wang, Y. M. Liu, *Biosens. Bioelectron.* **2014**, *55*, 195.
[120] A. Splendiani, L. Sun, Y. B. Zhang, T. S. Li, J. Kim, C. Y. Chim, G. Galli, F. Wang, *Nano Lett.* **2010**, *10*, 1271.
[121] X. R. Gan, H. M. Zhao, X. Quan, *Biosens. Bioelectron.* **2017**, *89*, 56.
[122] M. Sharma, A. Kumar, P. K. Ahluwalia, *RSC Adv.* **2016**, *6*, 60223.
[123] H. Vovusha, B. Sanyal, *RSC Adv.* **2015**, *5*, 67427.

[124] C. Lu, Y. B. Liu, Y. B. Ying, J. W. Liu, *Langmuir* **2017**, *33*, 630.
[125] S. J. He, B. Song, D. Li, C. F. Zhu, W. P. Qi, Y. Q. Wen, L. H. Wang, S. P. Song, H. P. Fang, C. H. Fan, *Adv. Funct. Mater.* **2010**, *20*, 453.
[126] X. Wang, F. Nan, J. Zhao, T. Yang, T. Ge, K. Jiao, *Biosens. Bioelectron.* **2015**, *64*, 386.
[127] Y. Huang, Y. Shi, H. Y. Yang, Y. Ai, *Nanoscale* **2015**, *7*, 2245.
[128] H. M. Deng, X. J. Yang, Z. Q. Gao, *Analyst* **2015**, *140*, 3210.
[129] C. F. Zhu, Z. Y. Zeng, H. Li, F. Li, C. H. Fan, H. Zhang, *J. Am. Chem. Soc.* **2013**, *135*, 5998.
[130] H. Zhang, Y. Ruan, L. Lin, M. Lin, X. Zeng, Z. Xi, F. Fu, *Spectrochim. Acta, Part A* **2015**, *146*, 1.
[131] F. Zhang, S. Y. Wang, J. W. Liu, *Anal. Chem.* **2019**, *91*, 14743.
[132] Y. Q. Wen, C. Peng, D. Li, L. Zhuo, S. J. He, L. H. Wang, Q. Huang, Q. H. Xu, C. H. Fan, *Chem. Commun.* **2011**, *47*, 6278.
[133] B. W. Liu, Z. Y. Sun, X. Zhang, J. W. Liu, *Anal. Chem.* **2013**, *85*, 7987.
[134] N. Varghese, U. Mogera, A. Govindaraj, A. Das, P. K. Maiti, A. K. Sood, C. N. R. Rao, *ChemPhysChem* **2009**, *10*, 206.
[135] J. Lee, Y. Yim, S. Kim, M. H. Choi, B. S. Choi, Y. Lee, D. H. Min, *Carbon* **2016**, *97*, 92.
[136] C. Lu, Z. C. Huang, B. W. Liu, Y. B. Liu, Y. B. Ying, J. W. Liu, *Angew. Chem., Int. Ed.* **2017**, *56*, 6208.
[137] A. Lopez, Y. Zhao, Z. C. Huang, Y. F. Guo, S. K. Guan, Y. Jia, J. W. Liu, *Adv. Mater. Interfaces* **2021**, *8*, 2001798.
[138] B. W. Liu, Y. Zhao, Y. Jia, J. W. Liu, *J. Am. Chem. Soc.* **2020**, *142*, 14702.
[139] W. H. Wu, Y. F. Fan, B. Tan, H. M. Zhao, *Microchim. Acta* **2020**, *187*, 608.
[140] Y. Yu, C. Yu, Y. Niu, J. Chen, Y. Zhao, Y. Zhang, R. Gao, J. He, *Biosens. Bioelectron.* **2018**, *101*, 297.
[141] X. X. Shi, H. M. Meng, X. Geng, L. B. Qu, Z. H. Li, *ACS Sens.* **2020**, *5*, 3150.
[142] P. Huang, J. Lin, S. J. Wang, Z. J. Zhou, Z. M. Li, Z. Wang, C. L. Zhang, X. Y. Yue, G. Niu, M. Yang, D. X. Cui, X. Y. Chen, *Biomaterials* **2013**, *34*, 4643.
[143] J. Lin, S. J. Wang, P. Huang, Z. Wang, S. H. Chen, G. Niu, W. W. Li, J. He, D. X. Cui, G. M. Lu, X. Y. Chen, Z. H. Nie, *ACS Nano* **2013**, *7*, 5320.
[144] Y. M. Liu, K. Ma, T. F. Jiao, R. R. Xing, G. Z. Shen, X. H. Yan, *Sci. Rep.* **2017**, *7*, 42978.
[145] J. Park, D. Q. Yuan, K. T. Pham, J. R. Li, A. Yakovenko, H. C. Zhou, *J. Am. Chem. Soc.* **2012**, *134*, 99.
[146] N. Yanai, T. Uemura, M. Inoue, R. Matsuda, T. Fukushima, M. Tsujimoto, S. Isoda, S. Kitagawa, *J. Am. Chem. Soc.* **2012**, *134*, 4501.
[147] S. Henke, A. Schneemann, R. A. Fischer, *Adv. Funct. Mater.* **2013**, *23*, 5990.
[148] L. Heinke, M. Cakici, M. Dommaschk, S. Grosjean, R. Herges, S. Brase, C. Woll, *ACS Nano* **2014**, *8*, 1463.
[149] F. Luo, C. B. Fan, M. B. Luo, X. L. Wu, Y. Zhu, S. Z. Pu, W. Y. Xu, G. C. Guo, *Angew. Chem., Int. Ed.* **2014**, *53*, 9298.
[150] S. S. Nagarkar, A. V. Desai, S. K. Ghosh, *Chem. - Asian J.* **2014**, *9*, 2358.
[151] F. X. Coudert, *Chem. Mater.* **2015**, *27*, 1905.
[152] L. L. Tan, H. W. Li, Y. C. Qiu, D. X. Chen, X. Wang, R. Y. Pan, Y. Wang, S. X. A. Zhang, B. Wang, Y. W. Yang, *Chem. Sci.* **2015**, *6*, 1640.
[153] X. S. Meng, B. Gui, D. Q. Yuan, M. Zeller, C. Wang, *Sci. Adv.* **2016**, *2*, e1600480.
[154] Z. Zhou, M. Vazquez-Gonzalez, I. Willner, *Chem. Soc. Rev.* **2021**, *50*, 4541.
[155] C. E. Chen, F. Pu, Z. Z. Huang, Z. Liu, J. S. Ren, X. G. Qu, *Nucleic Acids Res.* **2011**, *39*, 1638.
[156] C. H. Lu, I. Willner, *Angew. Chem., Int. Ed.* **2015**, *54*, 12212.
[157] Y. L. Li, P. R. Zhao, T. Gong, H. Wang, X. W. Jiang, H. Cheng, Y. Y. Liu, Y. L. Wu, W. B. Bu, *Angew. Chem., Int. Ed.* **2020**, *59*, 22537.
[158] Y. B. Nie, D. Li, Y. Peng, S. F. Wang, S. Hu, M. Liu, J. S. Ding, W. H. Zhou, *Int. J. Pharm.* **2020**, *585*, 119513.
[159] H. Zhang, P. Xu, X. Zhang, X. Cao, W. Han, M. Liu, X. Liu, W. Zeng, *Chin. Chem. Lett.* **2020**, *31*, 1083.
[160] Y. Yang, S. Zhong, K. Wang, J. Huang, *Analyst* **2019**, *144*, 1052.
[161] J. Liu, Y. Lu, *Chem. Commun.* **2007**, 4872.
[162] J. Liu, Y. Lu, *J. Am. Chem. Soc.* **2005**, *127*, 12677.
[163] J. W. Liu, Y. Lu, *Chem. Mater.* **2004**, *16*, 3231.
[164] J. W. Liu, Y. Lu, *J. Am. Chem. Soc.* **2004**, *126*, 12298.
[165] J. W. Liu, Y. Lu, *J. Am. Chem. Soc.* **2003**, *125*, 6642.
[166] X. Y. Xu, W. L. Daniel, W. Wei, C. A. Mirkin, *Small* **2010**, *6*, 623.
[167] X. Li, W. Yun, W. L. Guo, W. L. Zhang, L. Z. Yang, *Sens. Actuators, B* **2019**, *301*, 127170.
[168] P. W. Wu, K. V. Hwang, T. Lan, Y. Lu, *J. Am. Chem. Soc.* **2013**, *135*, 5254.
[169] L. Li, J. Feng, Y. Y. Fan, B. Tang, *Anal. Chem.* **2015**, *87*, 4829.
[170] C. Yang, X. Yin, S. Y. Huan, L. Chen, X. X. Hu, M. Y. Xiong, K. Chen, X. B. Zhang, *Anal. Chem.* **2018**, *90*, 3118.
[171] W. Wang, N. S. R. Satyavolu, Z. Wu, J. R. Zhang, J. J. Zhu, Y. Lu, *Angew. Chem., Int. Ed.* **2017**, *56*, 6798.
[172] M. R. Cui, X. L. Li, J. J. Xu, H. Y. Chen, *ACS Appl. Mater. Interfaces* **2020**, *12*, 13005.
[173] Y. A. Wu, J. Huang, X. H. Yang, Y. J. Yang, K. Quan, N. L. Xie, J. Li, C. B. Ma, K. M. Wang, *Anal. Chem.* **2017**, *89*, 8377.
[174] H. Y. Peng, X. F. Li, H. Q. Zhang, X. C. Le, *Nat. Commun.* **2017**, *8*, 14378.
[175] K. Chen, Q. Huang, T. Fu, G. L. Ke, Z. B. Zhao, X. B. Zhang, W. H. Tan, *Anal. Chem.* **2020**, *92*, 7404.
[176] C. Xu, F. Zhang, K. Wang, E. S. Xu, Y. Liu, W. Wei, S. Q. Liu, *Sens. Actuators, B* **2019**, *298*, 26930.
[177] C. Liu, Y. Hu, Q. Pan, J. Yi, J. Zhang, M. He, M. He, T. Chen, X. Chu, *Biosens. Bioelectron.* **2019**, *136*, 31.
[178] Z. Z. Yu, M. M. Wang, W. Pan, H. Y. Wang, N. Li, B. Tang, *Chem. Sci.* **2017**, *8*, 4896.
[179] N. Li, H. Yang, W. Pan, W. Diao, B. Tang, *Chem. Commun.* **2014**, *50*, 7473.
[180] R. C. Qian, Y. Cao, Y. T. Long, *Anal. Chem.* **2016**, *88*, 8640.
[181] H. Park, J. Kim, S. Jung, W. J. Kim, *Adv. Funct. Mater.* **2018**, *28*, 1705416.
[182] Z. M. He, P. H. Zhang, X. Li, J. R. Zhang, J. J. Zhu, *Sci. Rep.* **2016**, *6*, 22737.
[183] X. H. Zhao, R. M. Kong, X. B. Zhang, H. M. Meng, W. N. Liu, W. Tan, G. L. Shen, R. Q. Yu, *Anal. Chem.* **2011**, *83*, 5062.
[184] W. Yun, H. Wu, X. Y. Liu, M. Fu, J. L. Jiang, Y. F. Du, L. Z. Yang, Y. Huang, *Anal. Chim. Acta* **2017**, *986*, 115.
[185] A. Ravikumar, P. Panneerselvam, K. Radhakrishnan, *Microchim. Acta* **2018**, *185*, 8698.
[186] A. Mal, R. K. Mishra, V. K. Praveen, M. A. Khayum, R. Banerjee, A. Ajayaghosh, *Angew. Chem., Int. Ed.* **2018**, *57*, 8443.
[187] G. Das, F. Benyettou, S. K. Sharma, S. K. Sharama, T. Prakasam, F. Gandara, V. A. de la Pena-O'Shea, N. Saleh, R. Pasricha, R. Jagannathan, M. A. Olson, A. Trabolsi, *Chem. Sci.* **2018**, *9*, 8382.
[188] Y. Peng, Y. Huang, Y. Zhu, B. Chen, L. Wang, Z. Lai, Z. Zhang, M. Zhao, C. Tan, N. Yang, F. Shao, Y. Han, H. Zhang, *J. Am. Chem. Soc.* **2017**, *139*, 8698.
[189] W. Li, C. X. Yang, X. P. Yan, *Chem. Commun.* **2017**, *53*, 11469.
[190] Z. Qing, G. Luo, S. Xing, Z. Zou, Y. Lei, J. Liu, R. Yang, *Angew. Chem., Int. Ed.* **2020**, *59*, 14044.
[191] B. Hu, F. Kong, X. Gao, L. Jiang, X. Li, W. Gao, K. Xu, B. Tang, *Angew. Chem., Int. Ed.* **2018**, *57*, 5306.
[192] A. X. Li, J. Zhang, J. C. Qiu, Z. H. Zhao, C. Wang, C. J. Zhao, H. Liu, *Talanta* **2017**, *163*, 78.

[193] Y. L. Chu, B. Cai, Y. Ma, M. G. Zhao, Z. Z. Ye, J. Y. Huang, *RSC Adv.* **2016**, *6*, 22673.
[194] Y. X. Yuan, R. Q. Li, Z. H. Liu, *Anal. Chem.* **2014**, *86*, 3610.
[195] A. H. Loo, A. Bonanni, Z. Sofer, M. Pumera, *ChemPhysChem* **2015**, *16*, 2304.
[196] W. Ren, P. J. J. Huang, D. de Rochambeau, W. J. Moon, J. Y. Zhang, M. S. Lyu, S. J. Wang, H. Sleiman, J. W. Liu, *Biosens. Bioelectron.* **2020**, *165*, 112286.
[197] P. J. Huang, D. de Rochambeau, H. F. Sleiman, J. Liu, *Angew. Chem., Int. Ed.* **2020**, *59*, 3573.

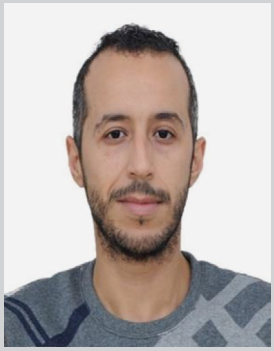

Jabrane Jouha obtained his Ph.D. in organic chemistry (2017) jointly supervised by the University of Orléans and the University Sultan Moulay Slimane in France and Morocco. After that, he joined the College of Chemistry and Chemical Engineering in Hunan University as the postdoctoral research associate during 2018–2020 under the supervision of Prof. Zebing Zeng. At present, he is a postdoc fellow of Prof. Hai Xiong group at the Institute of Advanced Study in Shenzhen University. His research interest includes the synthesis of novel therapeutic molecules, the design of organic π-frameworks and DNA nanomaterials for the detection of toxic analytes.

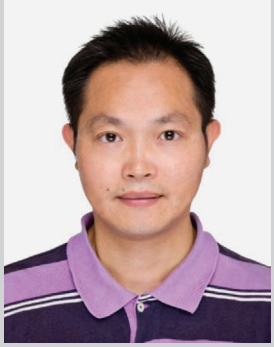

Hai Xiong is currently a Principal Investigator at the Institute of Advanced Study in Shenzhen University since 2016. He received Ph.D. in chemistry at Osnabrück University during 2006–2012. After that, he conducted a postdoctoral associate at the school of medicine in Yale University during 2012–2016. His research interest focuses on biomaterial-conjugated functional DNAzyme, supermolecular AIEgens, DNA hydrogel, DNA biosensors/cell imaging and lead investigator of many publications on different journals such as *J. Am. Chem. Soc., Angew. Chem. Int. Ed., Small, Nucleic Acid Res., Chem. Eng. J., Anal. Chim. Acta., Org. Lett., Chin. Chem. Lett., Bioconjugate Chem,* and *J. Org. Chem.*